JOURNAL OF SOLID STATE CHEMISTRY 2, 109–133 (1970)

Effect of Oxygen-Deficiency on Electrical Transport Properties of Tungsten Trioxide Crystals*

JAMES M. BERAK† AND M. J. SIENKO

Department of Chemistry, Cornell University, Ithaca, New York 14850

Received December 9, 1969

Single crystals of various substoichiometric tungsten trioxide crystals have been prepared by vapor phase transport and annealed under varying conditions. Electric resistivity, Hall voltage and Seebeck coefficient have been investigated as functions of temperature in the range 100–500°K and as functions of composition down to the compound $WO_{2.90}$. For stoichiometric WO_3, the results are in general agreement with previous reports. The jump in resistivity at the monoclinic–triclinic transition is due mainly to a decrease in electron mobility. The change at the triclinic-(low temperature) transition is almost entirely the result of a large decrease in the carrier concentration. Changes in thermoelectric power cannot be explained on the basis of the ordinary electronic component; a lattice contribution must be present. Removal of oxygen pushes the transitions to lower temperatures, increases the carrier concentration, decreases the Hall mobility, and changes the sign of its temperature dependence. Segregation of oxygen defects apparently occurs even for $x < 0.0001$ in WO_{3-x}, and it is believed that the basic defect unit is not the oxygen vacancy but the Anderson–Hyde disk of shear. The upper bound for this type of defect structure appears to be at $x = 0.013$. The increase of mobility with increasing temperature is attributed to hopping of charge carriers in place of band processes in the defect regions. Decreases in the optical phonon drag and transport energy terms are needed to fit the thermoelectric power behavior of the monoclinic phase. X-ray studies show essentially no change in the cell parameters for the reduced crystals. There is strong optical absorption in the red and near infrared associated with the oxygen deficiency, but only negligible paramagnetism. DTA studies show that the monoclinic-triclinic and triclinic-(low temperature) phase transitions are of the first-order and displacive type as in $BaTiO_3$; they are accompanied by transition heats of about 20 and 39 cal/mole, respectively. Measurements of resistivity and Seebeck coefficient on a $W_{20}O_{58}$ crystal suggest metallic-like behavior.

Introduction

The purpose of this work was to investigate the effect of small known amounts of oxygen deficiency on the electrical transport properties of single crystals of tungsten trioxide. Following the work of Sawada and Danielson (*1*) on the dc resistivity of WO_3 ceramics and crystals from room temperature to 1000°C, Crowder and Sienko (*2, 40*) studied the temperature dependencies of resistivity, Hall coefficient, and Seebeck coefficient on a single crystal from −70 to 600°C. In the monoclinic phase, which is stable from 17 to about 350°C, the temperature dependence of the Hall coefficient was found to be consistent with the excitation of electrons from shallow donor impurity levels 0.04 eV below the normally empty conduction band of tungsten trioxide, and the temperature dependence of the Hall mobility, with polar scattering by longitudinal optical-mode lattice vibrations. Both the perturbation theory of Howarth and Sondheimer (*3*) and the "intermediate-coupling" theory of Lee, Low, and Pines (*4*) were used to fit the data, leading to the following parameters: density-of-states effective mass, $m^* = 0.7\ m_0$, characteristic Debye temperature $\theta_l = 600$°K, polaron effective mass $m^{**} = 1.0$ to $1.1\ m_0$, effective mass $m^* = 1.2\ m_0$ to give best fit to perturbation theory with $\theta_l = 600$°K, and coupling constant $\alpha = 3$. Because α was greater than unity, the applicability of the perturbation theory was questioned, but with proper adjustment of the effective mass from $0.7\ m_0$ to $1.2\ m_0$ the observed

* This research was sponsored by the Air Force Office of Scientific Research through Grant #69-1726 and was supported in part by the National Science Foundation and the Advanced Research Projects Agency.

† Present Address: United Aircraft Research Laboratories, East Hartford, Connecticut.

mobility of about 16 cm^2/V sec could be rationalized. On cooling to the triclinic phase, which is stable between −40 and +17°C, there was a sharp decrease in Hall mobility (about a factor of 2), an increase in the Seebeck coefficient, and a slight increase in the Hall coefficient and its temperature dependence. The mobility change could be interpreted on the basis of polar scattering by optical phonons, but the Seebeck coefficient could not be explained solely by a change in effective mass. Additional scattering by acoustical mode piezoelectric phonons was suggested to account for the difference. The changes in the Hall coefficient were explained by a slight increase in donor ionization energy. Below −40°C, in what is called here the low-temperature phase, there was a marked increase in resistivity (about a factor of 100) which could be explained either through a large decrease in carrier concentration, or mobility, or both. An extra phonon-drag term was postulated to account for the large increase in Seebeck coefficient and its temperature dependence.

Crowder and Sienko also reported that a tungsten trioxide crystal that had been heated in vacuum to effect oxygen removal did not exhibit any discontinuities in resistivity and Seebeck coefficient at the phase transitions. The Hall and Seebeck coefficients were still negative but smaller in magnitude than before oxygen removal. The Hall mobility was reported to be insensitive to oxygen removal. Removal of oxygen from WO_3 to give lower oxides of tungsten has been reported by numerous investigators. Tungsten trioxide has a distorted ReO_3 structure, and appreciable removal of oxygen results in a partial breakdown of corner sharing to edge sharing for some octahedra. This occurs for the proposed structures, $W_{50}O_{148}$ and $W_{25}O_{74}$, $W_{40}O_{118}$, $W_{20}O_{58}$, $W_{18}O_{49}$, and W_4O_8. With the exception of the first structures the percentage of affected octahedra increases as more oxygen is removed. In this way, the approximately octahedral coordination of the tungsten atoms is retained, and no oxygen vacancies need be created in order to account for the increase in the tungsten-to-oxygen ratio. In W_4O_8 infinite strings of distorted octahedra are connected by edge sharing, and these strings are linked by way of corner sharing of the octahedra (*5*). In the case of $W_{20}O_{58}$, blocks of corner-sharing octahedra, which have an infinite extent in two dimensions and a characteristic width of twenty octahedra in the third, are mutually connected along folded planes where groups of six octahedra share edges (*6*). Magnéli has referred to the connecting regions as "recurrent dislocations" present in a normally corner-sharing octahedral network (*7*). According to Wadsley (*8*), these boundaries can be visualized as arising from the process of crystallographic shear along certain directions of the normal trioxide structure after removal of certain oxygen atoms. In $W_{20}O_{58}$ these shear planes are parallel to each other and have a characteristic period of almost 25 Å. Magnéli has suggested there might exist a homologous series of unit cell formula W_nO_{3n-2} each with a characteristic spacing between shear planes. $W_{40}O_{118}$, in which the separation between parallel shear planes is approximately 50 Å may be a member of this series (*9*, *10*). A related recurrent dislocation mechanism consisting of planes separated by about 30 Å has been advanced for $W_{50}O_{148}$ in which, to account for the stoichiometry $WO_{2.96}$, some tungsten atoms along the dislocation plane had to be coordinated to seven oxygen atoms (*11*).

For $x < 0.04$, no definite shear compounds of the Magnéli type have been characterized, partly because of difficulties in interpreting X-ray data in this range and partly because the equilibrium configuration of shear planes may be slow to form when the ordering principle has to be transmitted 50 Å and more. Past X-ray results have been interpreted in terms of either the random removal of oxygen atoms from the normal trioxide lattice (nonstoichiometry) or the existence of intermediate stoichiometric (Magnéli shear structures) or nonstoichiometric phases. According to Glemser and Sauer (*12*) the trioxide phase is nonstoichiometric and exists as such down to $WO_{2.95}$. More accurate limits have been set at $WO_{2.975}$ by Hägg and Magnéli (*13*) and at $WO_{2.98}$ by Choain and Marion (*14*). On the basis of small differences in the X-ray powder photographs, Hägg and Magnéli suggested the possibility that $WO_{2.975}$ (green) is a new phase that is very similar to tungsten trioxide. Gorbounova and Arslambekov (*15*) have interpreted their electron diffraction results in a similar manner in terms of the existence of two or more closely related oxide phases. On the other hand, Kellett and Rogers (*16*) concluded that strain and structural imperfection could account for the observed differences in their own X-ray results. Gebert and Ackerman (*11*) have indicated that it is possible for the trioxide phase to become "substoichiometric" down to about $WO_{2.98}$.

In terms of the shear plane concept nonstoichiometry can arise through a disordering of the shear planes by their being either nonparallel or aperiodic. The reduction of trioxide to $W_{20}O_{58}$ has been monitored with X-rays and has been interpreted in this way as involving an intermediate nonstoichiometric phase that possesses a random distribution of

shear planes (*17*, *18*). In the course of reduction the number of such shear planes increased, and under the particular experimental conditions (*18*), only at the composition $WO_{2.90}$ were the interactions between shear planes large enough to effect ordering.

Anderson (*19*) has outlined the steps that most likely occur in the process of forming Magnéli shear structures: (1) creation of oxygen vacancies at higher temperatures, (2) segregation of oxygen vacancies into arrays or dislocation lines, and (3) co-operative arrangement along planes of shear in order to eliminate oxygen vacancies and form Magnéli shear planes. In a dilute system containing very small amounts of oxygen deficiency, the shear planes may not be fully developed. The influence they have on electric and thermoelectric properties should give a more sensitive probe of ordering than do more conventional structural determinations.

Experimental Procedure

Materials

The ultra-pure tungsten trioxide powder used in this investigation was generously supplied by Dr. R. W. Mooney of Sylvania Electric Products, Towanda, Pennsylvania. Spectrographic analysis indicated the following impurity contents in parts per million: Al 0.6, Ca 2.0, Cr < 0.1, Fe < 3.0, Mg < 2, Mo < 10, Ni < 1, and Si < 18. As and Na were present at levels less than 0.8 ppm and 10 ppm, respectively; heavy-metal concentrations were less than 5 ppm. Reduction of the stoichiometric oxide was accomplished through use of the following gases which were obtained from and analyzed by the Matheson Co: O_2 (99.6%), Ar–O_2 mixture (0.95% O_2), Ar (99.998%), CO_2 (99.99%), CO_2–CO mixture (1.70% CO), and CO (99.5%).

Crystal Growth

Two methods were used to prepare crystals: (1) an indirect method in which single crystals of the stoichiometric oxide were grown and then selected crystals were annealed in a reducing atmosphere; (2) a direct method in which crystals were grown under a reducing atmosphere. Stoichiometric crystals for the indirect method were grown by the vapor-phase technique of Sawada and Danielson (*1*). A 50-g charge of tungsten trioxide was placed inside an inverted platinum crucible on a platinum sheet. Both platinum pieces were new and had previously been cleaned with boiling HCl in order to avoid possible iron contamination. Success of crystal growth depends on how well the platinum crucible seals to the platinum sheet at higher temperatures so as to prevent escape of tungsten trioxide vapor. The temperature was maintained at 1320 ± 20°C for eight days; subsequent cooling was at about 45°C per hour.

Small selected crystals (3-mm maximum length) were freed from ((110)) twinning by applying appropriate pressure with hand-held tweezers (*20*), and heated at 1022 ± 3°C for five days under a selected oxygen potential as determined by flow ratio of the various gases. The delivery system was checked by measuring the resistivity of a wire of CoO (*p*-type semiconductor) using the empirical relation of Duquesnoy and Marion (*21*). The crystals rested on a small sheet of platinum on the surface of a 2- to 3-g charge of tungsten trioxide powder. An external magnet assembly enabled rapid withdrawal of the samples so as to quench from 1022°C in 15 sec to 800°C, 1 min to 500°C, and 5 min to 190°C. After treatment the defect crystals varied from light green to black in overall appearance.

In the direct method of crystal preparation, a 20-g charge of tungsten trioxide was placed in the bottom of a quartz test tube that was mounted horizontally in an alumina combustion tube so that the closed end rested in the centre of a platinum furnace at about 1260°C and the open end, downstream of the gas flow at about 900 ± 100°C. Gas flow at manostat control pressure of 15–20 Torr for two days resulted in growth of large black crystals of defect oxide (up to 1 cm^2 in surface area) in the temperature gradient about halfway down the quartz tube. Most of the crystals studied in this investigation were prepared by the indirect method where the conditions of growth, annealing, and quenching were more precisely defined.

Chemical Analysis

The determination of oxygen deficiency was based on the method of Choain and Marion (*22*) in which a weighed sample of reduced oxide is dissolved in boiling aqueous K_2CO_3 in the presence of $Ag(SCN)_4^{3-}$. The digestion solution is made by mixing 20 ml of a solution containing 40 g of AgSCN and 300 g KSCN per liter with 10 ml of a solution saturated with K_2CO_3 and containing 0.3-*M* KCN. Powder samples dissolved in about 15 min, but even with vigorous stirring and crushing with glass beads on a magnetic hot plate crystal samples took up to 2 hr. Silver metal, precipitated in a quantity proportional to the total reducing power of the sample, was transferred onto the fritted disk of a Gooch filter crucible, washed with 2-*M* KSCN and then water, and then dissolved in 6-*M* HNO_3. After boiling down and cooling silver

was determined by the Volhard method through titration with 0.01 N KSCN using Fe^{3+} as indicator. The analysis method is capable of great precision, and the oxygen deficiency x in WO_{3-x} can be determined with great accuracy if one makes the following assumptions:

(1) The weight of sample analyzed is due only to the two components, tungsten and oxygen.

(2) The total electrochemical effects of other oxidizing or reducing elements is negligible compared to the effect produced by oxygen removal.

(3) There is no accidental or systematic loss of silver during analysis. Standardization of the analytical technique using known amounts of tungsten powder ($x = 3$) to produce 10, 30, and 80 μmole of precipitated silver disclosed in eighteen calibration experiments a systematic loss of about 2 μmole of silver, so this correction was applied to all samples. Sample size was chosen so as to keep the amount of precipitated silver under 100 μmole; for heavily reduced products, this required about 0.7 g of sample, but near stoichiometry, as much as 7 g of sample.

The oxygen deficiency of the small crystals from each annealing step was assigned on the basis of analysis of the powder that had been heated along with them. In order to test the validity of this assumption on a macroscopic level, an intimate mixture of small crystals and powder was annealed for one day at 1222°C in the presence of the 1.70% CO gas mixture. Separate duplicate analyses of the powder and crystals confirmed this assumption by giving the following identical results: powder, $x =$ 0.0121 and 0.0118; crystals, $x = 0.0117$ and 0.0121. In another annealing experiment powder was heated under identical conditions for five days, and duplicate analyses yielded $x = 0.0114$ and 0.0121 ± 0.003.

Electrical Measurements

Crystals that did not contain any ((110)) twinning were cleaved in air with a razor blade along the crystallographic a axis and freed from (100) twinning to various degrees by applying the appropriate shearing stress (*20*) with tweezers. In the detwinning process the (100) twin walls could not be completely removed, and some usually remained at the ends of the crystal. It became increasingly difficult to remove or induce these twin boundaries as x increased. As a result, some (100) twin planes remained throughout crystals that had moderate amounts of oxygen deficiency. In the heavily reduced samples crystals free of ((110)) twinning were not obtainable. Electric contacts to the crystals were obtained by utilizing the wetting action of In–Hg amalgam (for contacts below room temperature) or Ga metal (for contacts above room temperature).

Details of the crystal holders and measuring sequences are given elsewhere (*23*). Copper and platinum leads were used to measure potential drops due to IR, Seebeck, or Hall effects. Cooling was provided by a five-component organic mixture (chloroform, methylene chloride, ethyl-bromide, *trans*-1,2-dichloroethylene, trichloro-ethylene) or by liquid nitrogen. Precise regulation to 0.1°C of the temperature at the crystal was achieved by proportional control of the current through ¼-W carbon resistors situated below the crystal, using a Leeds–Northrup CAT controller and AZAR recorder.

Differences in potential were measured using an ac method with phase-sensitive lock-in amplifier or standard dc methods using a potentiometer or electrometer. The standard four-probe arrangement was used for specific resistivity. Contact separation and crystal cross-section were measured with a microscope having a stage micrometer calibrated, graduated ocular. Unless otherwise indicated, resistivity results are for current along the a axis with no twinning between the contacts at room temperature. Typical errors in resistivity were estimated to be $\pm$ 16%. Hall voltages were obtained by the ac method, using phase-sensitive detection of the signal between a fixed probe and a virtual probe on a potential divider. Dependence on magnetic field, systematically monitored in both directions, was linear to $\pm$ 2% in the 0 to 10,500-G range. The Hall voltage was independent of frequency and linearly dependent on current within $\pm$ 1% in the intervals 0.1–2.5 mA rms and 23–500 Hz. Seebeck coefficients were measured using the copper leads of the copper-constantan thermocouples. Unlike the resistivity and Hall coefficient measurements, the Seebeck values applied to crystal regions containing some (100) twin boundaries, at least near the ends of the crystal. The magnitude of the Seebeck coefficient was observed to be independent of the magnitude or direction of the temperature gradient to $\pm$ 3%. Temperature gradients used varied from 0.6–2.2°C.

X-Ray Diffraction

Powder and crystal diffraction experiments were done using a General Electric XRD-5 diffractometer and a Norelco XR-1 diffraction unit fitted with a Weissenberg rotation camera. In the diffractometer work Na_2MoO_4 was used as internal standard. For single-crystal photographs, crystals were aligned by the oscillation method of Davies (*24*). Nickel-

filtered CuKα radiation was used in all these experiments.

Optical Absorption

The optical absorption characteristics of crystals were obtained using Cary Model 14 and 15 recording spectrophotometers. For the measurements with unpolarized light in the visible and near infrared (up to 2 μ) a selected plate crystal was mounted in the Model 14 so that its c axis was approximately parallel to the incident beam. The absorption of visible light polarized along the a or b axis for a section of reduced crystal that was free from ((110)) twinning was similarly carried out on the Model 15 spectrophotometer. Corrections for reflections at the air-sample interfaces as well as for multiple reflections inside the crystal could not be made, so the results quoted below are only approximate.

Magnetic Susceptibility

The magnetic susceptibility of one reduced sample was measured by the Gouy method over the temperature range 1.3–300°K. The magnet and cryogenic system have been described elsewhere (*25*).

DTA

Differential-thermal-analysis studies were carried out on single crystals using the calorimeter and electronic equipment described elsewhere (*26*). The calorimeter consisted of an insulated cylindrical aluminum block in which reference and sample wells had been formed and which could be by cooled flowing liquid nitrogen through encircling copper coils or heated by supplying current to a wire-wound tubular heater placed along the cylindrical axis. Two Pyrex compartments, each containing two copper-constantan thermocouples embedded in a soft glass probe, were constructed as similarly as possible and inserted into these wells, where aluminum powder served as heat exchanger with the aluminum block. The reference junctions of the thermocouples were maintained at the sublimation point of carbon dioxide. One of the thermocouples from the sample compartment led to one input of a two-channel strip-chart Honeywell recorder. The other sample thermocouple and one reference thermocouple were connected in series so that the net emf was approximately zero. After amplification by a microvolt-ammeter, this emf was simultaneously applied to the second channel of the Honeywell recorder. With a crystal held at the tip of the soft-glass probe close to the thermocouples by a small amount of Apiezon T grease and with nothing additional in the reference compartment, any anomalies in the specific heat at a phase transition could be detected. Integration of the recorder pen deflection with respect to the base line was accomplished with a planimeter.

In separate experiments a calibration of the apparatus was obtained by recording the latent heat at the melting and freezing points of small drops of mercury. The maximum sensitivity of the apparatus was established at 0.1 μcal. For a given mercury drop the measured areas of heating and (usually supercooled) cooling peaks agreed with each other to $\pm$ 3/2% and were independent of the thermal rates (0.8–2.5°C per min). However, a 9% decrease in heat detected per mole was recorded as the weight of the mercury drop increased from 38–282 μg, probably because of heat loss through an air path. Consequently, calibration was based on the smaller mercury drops for which linear dependence on sample weight was the rule.

In the crystal experiments the number of microcalories of heat detected per micromole of crystal also depended on the sample weight and was independent of the heating and cooling rates. In the case of single crystals of tungsten trioxide a 30% drop in the transition heat per mole was observed as the weight of crystal increased from 49–330 μg. This effect of the extra air path on the efficiency of heat collection at the thermocouple is therefore a relatively large one. In the analysis of the data its magnitude will be reduced by comparing the transition heats only of crystals with similar weights. Weights of all crystals and mercury pools are accurate to $\pm$ 1 μg and were obtained through use of a Cahn electronic balance.

Results and Discussion

X-Ray Diffraction

In the powder measurements all the observed peaks up to $2\theta = 60$°C for a sample of composition $WO_{2.9873\pm0.0003}$, which was annealed under a CO_2/CO ratio of 58, and for the WO_3 starting material could be identified according to the indexing procedure of Magnéli et al. (*27*) for tungsten trioxide. The parameters obtained are: WO_3—$a = 7.302 \pm 0.003$ Å, $b = 7.538 \pm 0.003$ Å, $c = 3.845 \pm 0.0015$ Å, and $\beta = 90.83 \pm 0.03°$; $WO_{2.9873}$—$a = 7.302 \pm 0.0045$ Å, $b = 7.536 \pm 0.0045$ Å, $c = 3.850 \pm 0.0025$ Å, and $\beta = 90.80 \pm 0.05°$. With the possible exception of the c axis, the results of the powder work indicate that the unit-cell parameters are the same for the two compositions.

Single crystal rotation photographs were taken along the *a*, *b*, and *c* axes of two crystals of composition $WO_{2.99991\pm0.00002}$ [twinned (100)] and $WO_{2.9881\pm0.0003}$ [twinned ((110)) and (100)]. Although there was matching of the diffraction spots along layer lines for the corresponding rotation axes, the spots for the more reduced crystal were considerably broadened compared to the other crystal. Rotation photographs taken along the *c* axis exhibited the first- and third-order layer lines for both crystals. This agrees with previous findings (*11*, *28*) that the *c* axis as obtained from the powder work must be doubled. The single-crystal parameters observed in this work are: $WO_{2.9991}$—$a = 7.32 \pm 0.01$ Å, $b = 7.54 \pm 0.01$ Å, $c = 7.71 \pm 0.02$ Å; $WO_{2.9881}$—$a = 7.32 \pm 0.01$ Å, $b = 7.54 \pm 0.01$ Å, $c = 7.71 \pm 0.02$ Å. Within the rather large experimental error the results for the two compositions are identical and agree with both the powder work of this investigation and the literature values. However, the parameters for the more reduced oxide disagree with those advanced by Gebert and Ackermann (*11*) for $WO_{2.98}$. According to Gebert and Ackermann the powder diffraction at this composition was very similar to that of tungsten trioxide, but the *d* spacings suggested a relatively large increase in the unit-cell parameters.

In summary, the X-ray results of this investigation can be interpreted as indicating disorder since the unit-cell parameters are about the same as the trioxide and the diffracted beams are broadened. The region of nonstoichiometry, which could be caused by the formation of oxygen vacancies or lines and planes of shear, would, therefore, have as its lower boundary the composition $WO_{2.9873\pm0.0003}$.

Microscope Studies

Although the oxygen-deficient crystals appeared uniformly green or black under the relatively low magnification of a binocular microscope, green fringes or lines in the *ab* crystal plane ($x < 0.005$) were always observed against the normally yellow background of tungsten trioxide whenever the higher magnification of a Leitz petrographic polarizing microscope was utilized. These lines, having width less than about 0.5 μ, generally crisscrossed at an angle of $51.8 \pm 0.2°$, and the *b* axis bisected this angle. In the initial stages of reduction the lines were short and sometimes wavy; as reduction proceeded, the straight-line pattern was stabilized and extended. The green lines separated blocks of yellow trioxide-like material and appeared to define planes parallel to the *c* axis. At about the composition $WO_{2.9998}$ another straight-line pattern appeared with lines at $27.4 \pm 0.4°$ with respect to the *a* axis. On further reduction lines would merge into bands until finally at about the composition $WO_{2.995}$ the crystals became too opaque to be viewed by transmitted light.

From the orientations of both kinds of defects with respect to the crystallographic axes, the indices of their directions in order of appearance are known to be [[120]] and [[210]]. The [[120]] directions are ideally situated 25.85° with respect to the *b* axis; [[210]] are ideally oriented 27.3° with respect to the *a* axis.

In the case of viewing the *ac* crystal plane under high magnification a line defect that made an angle of $17.8 \pm 0.4°$ with respect to the *c* axis appeared at about the composition $WO_{2.9988}$. As the W/O ratio increased, their number also increased. Whether these dark lines had any small *b* component to their direction was difficult to determine; to a good approximation they can be regarded as lying in the *ac* plane and having indices [103] and [10$\bar{3}$]. With $a = 7.302$, $c = 7.70$ and $\beta = 90.8°$, these directions should make angles of 17.47° and 17.62° with respect to the *c* axis.

The appearance of short dark lines in trioxide crystals annealed in vacuum at 610°C has been reported by Horie and Iwai (*29*). These lines were reported to be confined only to the crystal surface and had the same orientation as the [[120]] line defects observed in this investigation. In addition, these authors (*29*, *30*) reported the presence of green bands in crystals that had been annealed above 330°C in the presence of zinc vapor. These bands were parallel to the (342) and (34$\bar{2}$) crystal planes and probably resulted from zinc entry into the trioxide lattice rather than from oxygen loss.

The effect of oxygen deficiency on the motion of a (110) twin plane differed from that of a (100) plane. Even in the case of very small oxygen deficiency ($x < 0.0001$) the movement of a (110) boundary under externally applied pressure was very difficult to accomplish. Usually the oxygen-deficient crystal would shatter under the high stresses without boundary movement. For this reason the crystals on which electrical measurements were carried out were prepared from larger defect crystals that were free from ((110)) twinning. The movement of (100) twin planes was possible down to about the composition $WO_{2.9988}$.

The above patterns were observed in cleaved and uncleaved crystals so are properties of the bulk material. Reoxidation in air at ca. 650°C eliminated all traces of these defects. There is little doubt that

removal of oxygen is directly responsible for the observed patterns. Essentially all the oxygen loss is concentrated along specific crystal directions. This segregation, which may be the beginnings of compound formation, could be accomplished at the temperatures of annealing or growth or during the cooling process. Since the preparation involved heating in the tetragonal phase, where [[120]] and [[210]] are indistinguishable, there should be no reason why one orientation should be favored at room temperature if segregation occurred only in this phase. The exclusive appearance of [[120]] for low values of oxygen deficiency points to considerable organization of simpler oxygen defects or reorganization of more complex defects on cooling below the orthorhombic-tetragonal transition temperature (710°C).

If compounds do precipitate on cooling, the most likely candidates are the Magnéli shear planes. Postulated homologous series include M_nO_{3n-1} and M_nO_{3n-2}, involving respectively groups of four and six edge-sharing octahedra along the shear planes. In both series compounds can be generated (*31*, *32*) by periodic removal of certain parallel planes of oxygen atoms from the trioxide structure and collapse of the corner-sharing octahedra to edge sharing along these planes. The removal of every n-th oxygen plane, which is parallel to the crystal planes that have Miller indices 0, 1, and j or $\bar{j}$, or any permutation of these, is required to generate the series M_nO_{3n-1} ($j = 2$) or M_nO_{3n-2} ($j = 3$). Since the observed line patterns [[120]], [[210]], [103], and [10$\bar{3}$] have the proper orientations with respect to the trioxide lattice to generate these Magnéli series, there is reason to believe that compound formation may be occurring along these defects. However, compound formation requires that the shear planes be periodic, parallel to each other, and infinite in two dimensions, criteria which cannot be assumed since the X-ray data indicate considerable disorder. It is more likely that there are parallel aperiodic shear planes, e.g., [120] ,of various sizes within a particular defect region. If so, definite compounds cannot be characterized, and a defect model (nonstoichiometry) would be a more appropriate description. Since segregation of oxygen defects was observed even for $x \sim 0.0001$, it must be concluded that the basic defect at room temperature is not the oxygen vacancy but is the shear discontinuity. These finite shears would then be oriented in specific crystal directions and definite planes which in order of appearance are ((210)), ((120)), and probably (301) and (30$\bar{1}$).

Anderson and Hyde (*31*, *32*) have postulated a mechanism for shear-plane formation which is as follows: In the initial stages of reduction there exists a small concentration of anion point defects. As reduction proceeds, oxygen vacancies aggregate into disks which have the proper orientations so that lattice shear occurs and the oxygen vacancies are eliminated. Since the shear planes terminate within the crystal, dislocation rings appear at the new boundaries with the trioxide lattice. Due to the resulting strain these boundaries act as traps for other vacancies, and on further removal of oxygen the small discs of shear grow into larger planes which extend throughout the crystal. In the case of WO_{3-x}, on slight reduction small concentrations of oxygen vacancies exist at the temperature of annealing in equilibrium with the oxygen potential of the reducing atmosphere. During the quenching process there is not enough time for the elimination of oxygen vacancies so that these agglomerate into orientations for which shear of the M_nO_{3n-1} type (four octahedra) can take place. Trioxide and defect regions are, therefore, observed at room temperature. As reduction proceeds, the density and size of the defect regions increase. Eventually the density of oxygen vacancies at the temperature of annealing becomes high enough that shear involving six octahedra (M_nO_{3n-2} series) takes place during cooling.

Optical Absorption

Visible and near infrared absorption was monitored on crystals having O/W ratios of 3, 2.999925 ± 0.000035, and 2.99991 ± 0.00002 corresponding to Hall carrier concentrations of 2.4, 5, and 6.5×10^{18} electrons per cc, respectively. Both reduced crystals exhibited [[120]] patterns. All crystals contained (100) twin boundaries, but only the trioxide crystal was freed of ((110)) twinning by applying pressure. Crystal thicknesses were of the order of 0.02 cm.

Figure 1 shows the uncorrected optical density per cm path of crystal as a function of wavelength. The strong absorption edge near 2.7 eV is attributed to an allowed transition corresponding to excitation of an electron from the top of a filled band formed mainly of oxygen orbitals to the bottom of an ideally empty band composed largely of tungsten 5*d* orbitals (*33*). The nature of the absorption in the near infrared region of tungsten trioxide is not clear. Aside from ligand-field transitions, which are usually of low intensity, the observed decrease in optical transmission could be part of a broad absorption peak associated with excitation of electrons into the conduction band from donor levels in the forbidden gap or it could be attributed to

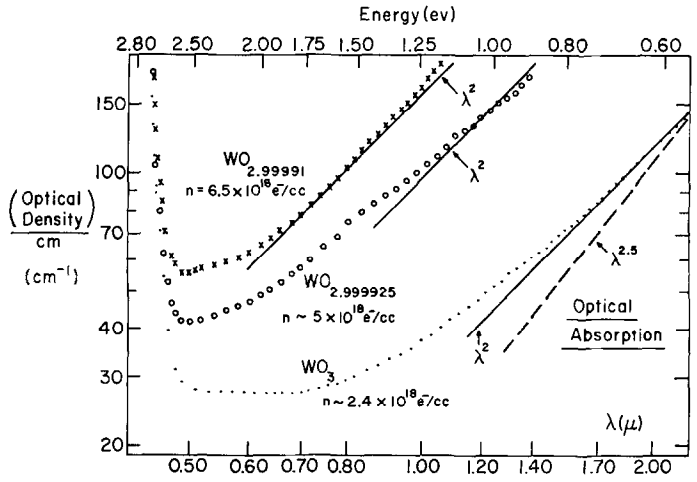

FIG. 1. Optical absorption versus wavelength for three crystals varying in W/O ratio.

transitions of thermally excited electrons within the conduction band. In the limit of high frequencies, assuming index of refraction does not vary with wavelength, the coefficient for free carrier absorption should increase as λ^2 (*34*). In case the electron is scattered by longitudinal optical-mode phonons, the dependence is modified slightly to $\lambda^{2.5}$ (*35*). The fact that the observed dependence approaches a quadratic at longer wavelengths may be an indication of free carrier absorption.

As oxygen is removed from the structure, the absorption increases at all wavelengths; this is especially apparent in the red and near infrared. The green color associated with the [[120]] line patterns can therefore be assigned to two absorptions which are maximized in the visible region at red and blue. The strong absorption in the blue is due to charge transfer across the forbidden gap; the absorption in the red, as with tungsten trioxide, may be due to photoexcitation of carriers into the conduction band or to free carrier absorption. Free carrier absorption should be enhanced in the regions of maximum lattice disturbance (along green lines) as a result of (1) a greater breakdown of the selection rules that forbid this transition and (2) an increase in carrier concentration.

When examined for absorption of polarized light in the *ab* plane, the portion of the $WO_{2.99991}$ crystal that did not contain ((110)) twinning showed a considerably higher optical density for polarization parallel to the *a* axis than for polarization parallel to the *b* axis. The anisotropy confirms the visual observation that the absorption associated with the [[120]] patterns is greater for *a*-axis polarized light. A slight dichroism in the fundamental absorption edge was also evident in agreement with a previous report (*36*) on WO_3 in which the absorption edge for *b*-polarized light is at higher energy than that for *a*-polarized light.

Electrical Resistivity of WO_3

Four stoichiometric crystals grown by the platinum crucible technique were examined. These are designated 11*b*, 11*a*, 11*aa*, and 8*a*. Crystals 11*b*, 11*a*, and 8*a* were free from twinning between the resistivity probes but did contain some (100) boundaries at their ends. Crystal 11*aa* was extensively twinned (100) along its entire length and was purposely made so by heating the crystal just above the monoclinic-orthorhombic transition temperature and quickly cooling to room temperature. Figure 2

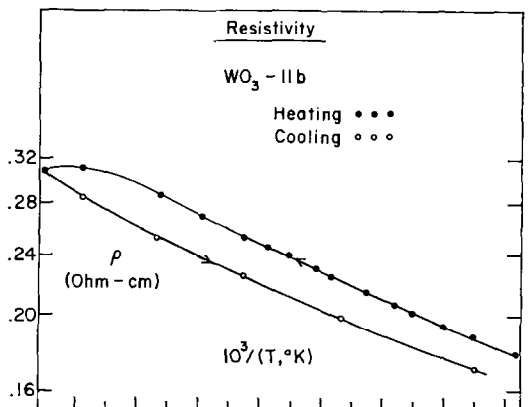

FIG. 2. Logarithm of the resistivity of a WO_3 crystal as a function of reciprocal temperature above room temperature.

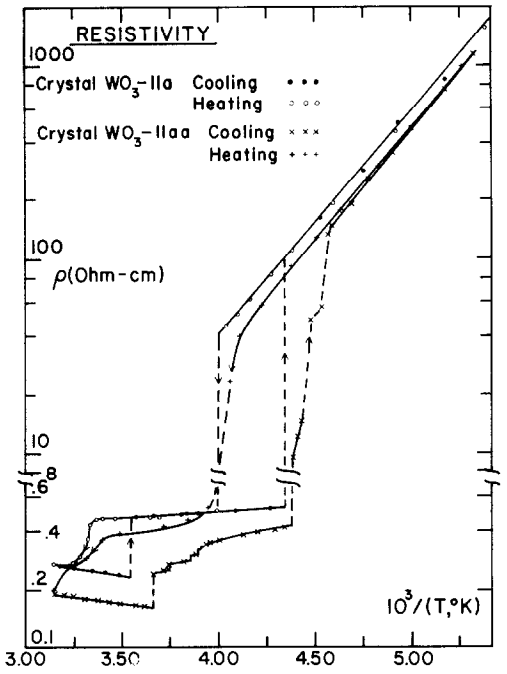

FIG. 3. Logarithm of the resistivity of WO_3 crystals as a function of reciprocal temperature below room temperature. Crystal 11*aa* was extensively twinned (100) along its entire length.

shows the course of resistivity versus reciprocal temperature for crystal 11*b* above room temperature. The temperature dependences on heating and cooling are similar, but there is a displacement to lower resistivity values on cooling. Since the Hall mobility for this crystal during heating roughly followed the same curve during cooling (see Fig. 6), the observed irreversibility is due solely to an increase in carrier concentration, probably because of slight diffusion of the gallium wetting agent into the WO_3 matrix at higher temperature.

Below room temperature the resistivities of untwinned and twinned crystals are shown in Fig. 3. The untwinned crystal on cooling shows at the monoclinic-triclinic and triclinic-(low temperature) transitions single jumps in resistivity by a factor of 2 and 200 at 9 and −43°C, respectively. On heating, the resistivity changes occur at higher temperatures; the low-temperature transition at −23°C was sharp but the following transition was spread out over a 10°C temperature interval just above room temperature. Such hysteresis effects with tungsten trioxide have been reported many times previously. For the crystal initially twinned at room temperature a marked step character is associated with all the transitions. This is attributable to the fact that various regions (domains) undergo transition at slightly different temperatures.

If the complicating effects of twinning are ignored, the agreement of resistivity values among crystals is good. The accuracy of these values is $\sim \pm 20\%$ and is sufficient to bring resistivity values into coincidence. The general slopes of all the curves are also in good agreement; for example, the activation energy for conduction in the low-temperature phase is 0.23 eV. This exponential dependence continues to temperatures at least as low as 150°K, where measurements became unreliable. Based on extrapolation, the resistivity at 80°K is estimated to be $10^9\ \Omega$ cm.

Hall Studies on WO_3

For presenting the data on the Hall coefficient, $R_H = rB/Nq \sim 1/nq$, it is assumed that the scattering-mechanism constant r and the band-shape parameter B are equal to unity at all temperatures. Figures 4 and 5 give the derived electron concentrations n as a function of reciprocal temperature for the crystals previously referred to in Figs. 2 and 3. Activation energies for carrier generation in the monoclinic phase are: crystal 11*b*, 0.0110 ± 0.0015 eV on heating and 0.0115 ± 0.0020 eV on cooling; crystal 11*a*, 0.015 ± 0.004 eV; and crystal 11*aa*, 0.016 ± 0.005 eV. The activation energy in the triclinic phase of crystal 11*a* is 0.031 ± 0.004 eV.

The ionization energy (E_d) of a single donor state cannot be obtained directly from Figs. 4 and 5 because the temperature dependence of the density of states in the conduction band (N_c) cannot be neglected when n is weakly dependent on temperature and because the degree of compensation by

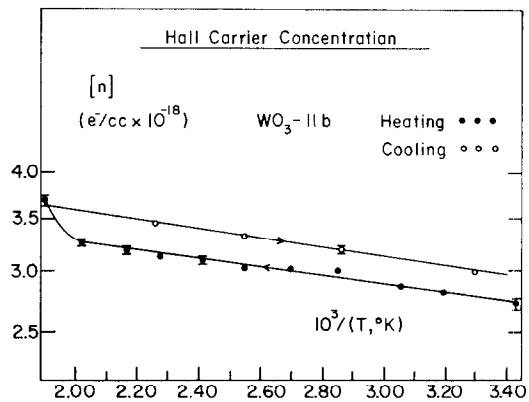

FIG. 4. Electron concentration versus reciprocal temperature as determined from Hall voltage measurements on a WO_3 crystal above room temperature.

acceptor states is not known. The donor ionization energy can be determined using the relation (*37*).

$$\frac{(n+N_a)\exp(\eta)}{(N_d-N_a-n)} = g^{-1}\exp(-E_d/kT), \qquad (1)$$

where η is the reduced Fermi level, E_F/kT, N_d, and N_a are the donor and acceptor concentrations, respectively, and g is the degeneracy of the donor level. Under the assumption that the (spin) degeneracy is 2 and that N_a is negligible, analysis of the data for crystal 11*b* gives $N_d = 3.9 \times 10^{18}$/cc, $E_d = 0.009$ eV, and $m^* = 0.84$. The ionization energy is considerably smaller than the 0.04 eV previously reported (*2*) for a crystal with $N_d = 1.9 \times 10^{18}$/cc and $m^* = 0.9$ m. Since the density-of-states effective masses are similar, the discrepancy in E_d is in accord with broadening of the impurity levels through overlap of their wave functions. Mott (*38*) has predicted that hydrogen-like donor states should overlap and E_d should drop to zero when the donors are separated by a distance roughly equal to 4.5 times the donor radius. Analysis for tungsten trioxide, using an effective dielectric constant (*2, 39*), indicates that critical overlap is being approached for $N_d \sim 2$ to 4×10^{18}/cc.

At the monoclinic-triclinic transition, as evidenced by crystal 11*a*, there is a small decrease in n as well as an increase in the activation energy for carrier generation. These observations agree with those reported previously (*2, 40*) and are consistent with an increase in E_d in the triclinic phase.

The only measurements of n in the low-temperature phase of WO_3 were obtained on crystal 8*a*. At the triclinic-(low temperature) transition n decreased by a factor of 230, which more than accounts for the observed factor of 170 increase in the resistivity. The activation energy for conduction in the low-temperature phase is 0.23 eV; an activation energy for carrier generation is calculated to lie between 0.21 and 0.28 eV.

Figures 6, 7, and 8 show how the calculated Hall mobility, $\mu_H = \sigma R_H$, varies with temperature in the stoichiometric WO_3 crystals studied. For all the crystals μ_H in a given phase increases as the temperature is lowered, as is characteristic of electrons in interaction with lattice vibrations. Because of the low values of μ_H, it is expected that coupling to optical modes predominates in the temperature interval considered. The magnitude and temperature dependence in the monoclinic phase can be explained on the basis of the slightly modified perturbation theory of Howarth and Sondheimer (*3*) and the large-polaron intermediate-coupling theory of Lee, Low, and Pines (*4*). The formation of a large-polaron band in WO_3 is reasonable because the mobility values shown in Figs. 6, 7, and 8 are greater than unity and because the polaron radius (r_p), which can be approximated

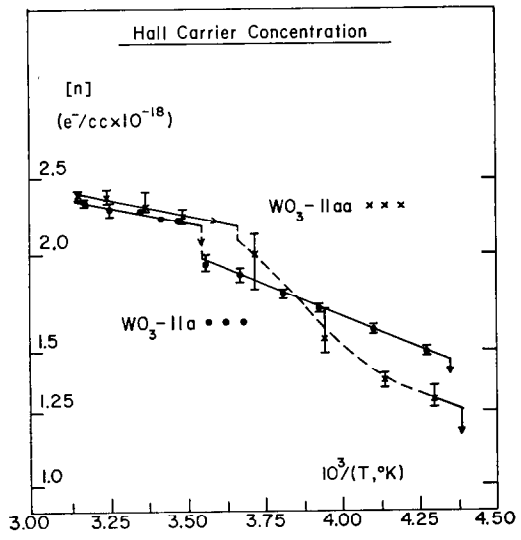

FIG. 5. Electron concentration versus reciprocal temperature below room temperature. Crystal 11*aa* was extensively twinned (100) along its entire length.

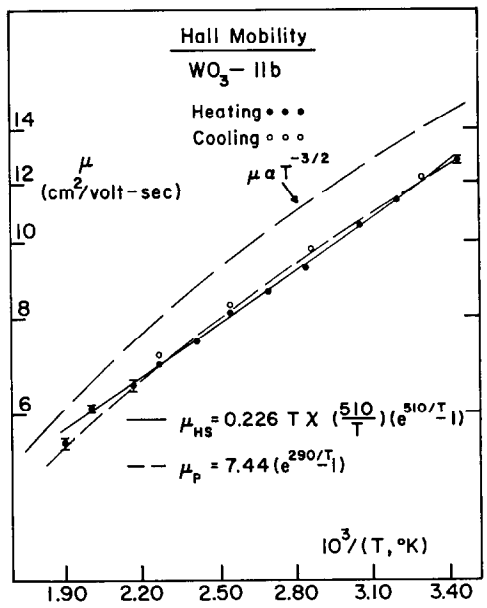

FIG. 6. Hall mobility versus reciprocal temperature for a WO_3 crystal above room temperature. Uppermost curve shows $T^{-3/2}$ dependence expected for scattering by acoustical modes. Lower curves show fit with optical-mode scattering theories of Howarth and Sondheimer (HS) and the large-polaron intermediate-coupling theory of Lee, Low, and Pines (P).

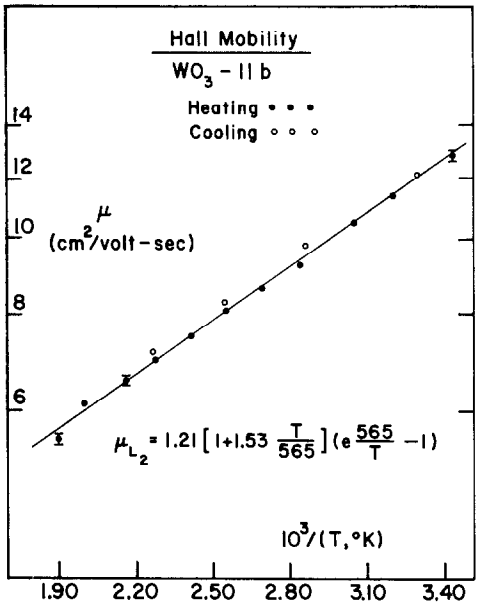

FIG. 7. Hall mobility versus reciprocal temperature for a WO_3 crystal below room temperature. Solid line is for Langreth theory of large-polaron mobility at relatively high temperatures.

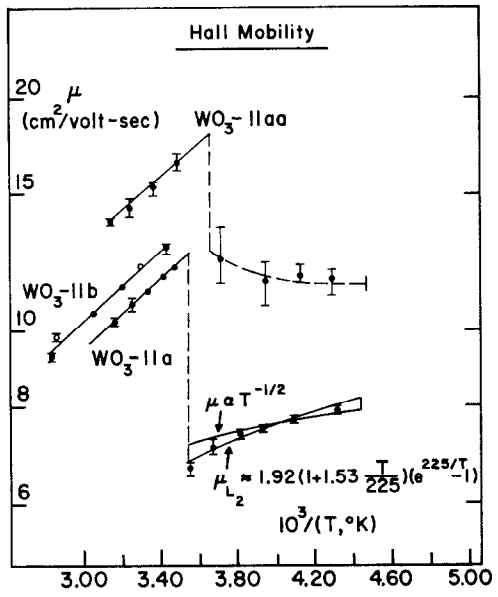

FIG. 8. Hall mobility versus reciprocal temperature for several crystals around the monoclinic-triclinic transition. Crystal 11*aa* has both phases so low-temperature portion could not be analyzed. Crystal 11a in triclinic phase is close to $T^{-1/2}$ or Langreth large-polaron model.

as $\hbar\,(2m^*k\theta_l)^{-1/2}$, is sufficiently large (8.5 Å) compared to the separation between tungsten atoms (3.8 Å).

In fitting the observed mobility values by the various theories, the important parameters to be obtained are the characteristic temperature of the longitudinal optical modes (θ_l), the coupling constant (α), the band effective mass (m^*), and the polaron effective mass (m^{**}). Table I summarizes the values of these parameters as deduced for the various mobility models. In the limit of weak coupling, the perturbation theory of Howarth and Sondheimer (HS), as reformulated by Petritz and Scanlon (*41*) leads to

$$\mu_{HS} = \frac{q\hbar}{2m^*\alpha k\theta_l}\frac{8}{3\pi^{1/2}}\frac{\chi(Z)\,[\exp(Z)-1]}{Z^{1/2}}, \quad (2)$$

where $Z = \hbar\omega_l/kT = \theta_l/T$ with ω_l equal to the characteristic vibrational frequency of the optical mode. $\chi(Z)$ is a slowly varying function which decreases from 1 to 0.66 as Z increases from zero to about 1.2 and then increases back to one as Z continues past 3. This perturbation approach holds for any temperature and formally requires that α must be much smaller than one, although it is believed (*42*) that the theory is still applicable for $\alpha \cong 1$. The coupling constant α, which is defined (*43*) as $(q^2/\hbar)(m^*/2\hbar\omega_l)^{1/2}(K_0^{-1} - K_s^{-1})$ with q equal to the charge and K_0, K_s the optical and static dielectric constants, respectively, is approximately equal to 3 for monoclinic tungsten trioxide. The Lee, Low, and Pines (LLP) large-polaron model

TABLE I

PARAMETERS FOR MONOCLINIC STOICHIOMETRIC WO_3 AS DERIVED FOR THE VARIOUS MOBILITY THEORIES

Mobility theory	Characteristic temp. θ_l (°K)	Coupling constant α	Effective masses m^*/m	m^{**}/m
HS	510	2.82	1.39	—
HS	(600)[a]	(2.9)	(1.2)	—
LLP	290	2.31	0.5	0.75
LLP	(600)	(2.2)	(0.7)	(1)
L_1	290	2.85	0.8	1.2
LK	290	2.56	0.65	1.15
W	290	2.61	0.7	1.0
S	290	3.93	1.55	3.8
Ō, K	290	2.57	0.65	1.1
L_2	565	3.00	1.75	3.26

[a] Parenthetic values are taken from Ref. (*32*) for crystal *RH* 14.

and others derived from it are useful for α at least as high as three. The LLP relation is

$$\mu_{LLP} = (q\hbar/2m^* \alpha k\theta_l) f(\alpha) (m^*/m^{**})^3 [\exp(Z) - 1], \quad (3)$$

where $f(\alpha)$ is a function which increases from 1 to 1.35 as α increases from 0 to 6 and $(m^{**}/m^*) = 1 + (\alpha/6)$. Langreth ($L_1$) replaces the exponent of the effective mass ratio by 1 (*44*). Weijland (W) gives a mobility equation similar to Langreth's except that an extra factor $(1 + 0.06\,\alpha)$ appears in the denominator (*45*). Langreth and Kadanoff (*46*) (LK) derive the same expression as μ_{L_1} except that $(m^{**}/m^*) = [1 - (\alpha/6)]^{-1}$. All four of these results, LLP, L_1, W, and LK are valid only for $T \ll \theta_l$.

Another general formulation of the polaron problem is due to Feynman (*47*), who treats the electron-lattice interaction as a harmonic-oscillator problem in which the electron is coupled to a fictitious particle representing the lattice. This model is the basis for the low-temperature mobility relations of Schultz (S) (*48*), Ōsaka (Ō) (*49*), and Kadanoff (K) (*50*).

The temperature dependence of the mobility in the LLP- and Feynman-based mobility equations can be put in the form,

$$\mu_p = D_p[\exp(\theta_l)_p/T - 1], \quad (4)$$

where D_p is a constant. Equation (2) can be rewritten as

$$\mu_{HS} = D_{HS} T^{1/2} \chi\left[\frac{(\theta_l)_{HS}}{T}\right]\left[\exp\left(\frac{(\theta_l)_{HS}}{T}\right) - 1\right]. \quad (5)$$

The temperature dependence of the data in the monoclinic phase of crystal 11*b* (see Fig. 6) best fits these relations if $(\theta_l)_p = 290°K$ and $(\theta_l)_{HS} = 510°K$.

Table I also includes for comparison the results of the analysis of Crowder (*51*) for his WO_3 crystal *RH* 14. Insofar as the values of the mobilities, coupling constants, and effective masses are concerned, the vapor-deposited crystal 11*b* of this investigation can only be favorably compared with his bulk-grown crystals, one of which is exemplified by *RH* 14. The discrepancies in θ_l most likely result from the different accuracies of measurement; there is a greater scatter in the mobility plot for crystal *RH* 14 than for 11*b*. The discrepancies in the values of θ_l between models is not surprising. Formally, all the mobility expressions, when applied to WO_3 in this temperature range, are on shaky grounds since $\alpha = 2.8$ and $(\theta_l)_p = 290°K$.

Recently, the problem of the large-polaron mobility at finite temperatures has been treated by Langreth (L_2) (*52*), who calculates that

$$\mu_{L_2} = \frac{q\hbar}{2m^* \alpha k\theta_l}\left(\frac{m^*}{m^{**}}\right)\left(1 + \frac{1.53}{Z}\right)[\exp(Z) - 1] \quad (6)$$

in which

$$(m^{**}/m^*) = (1 - 0.0008\,\alpha^2)\Big/\left(1 - \frac{\alpha}{6} + 0.0034\,\alpha^2\right). \quad (7)$$

These equations are claimed to be reasonably valid for α as high as 3 and for temperatures as high as $(\theta_l)/2$, a great improvement over the $T \ll \theta_l$ restriction of previous treatments. Equation (6) best fits the mobility data of crystal 11*b* when $\theta_l = 565°K$ and $\alpha = 3.00$; this curve is shown as the solid line in Fig. 7 where the logarithm of μ_{L_2} is plotted using

$$\mu_{L_2} = 1.21\left(1 + \frac{1.53T}{565}\right)\left[\exp\left(\frac{565}{T}\right) - 1\right]. \quad (8)$$

The derived parameters are listed as the last entry in Table I. The band mass, 1.75 m, which is higher than that of any of the previous analyses, and the polaron mass, 3.26 m, are probably the most accurate parameters.

If the electron interacts with only one optical mode in the triclinic phase, it is evident from the difference in slopes of the Hall mobility versus temperature for crystal 11*a* that the characteristic temperature of that optical mode must be substantially less than 565°K, the value in the monoclinic phase. The best fit to the polaron mobility expression of Langreth leads to

$$\mu_{L_2} = 1.92[1 + (1.53T/225)][\exp(225/T) - 1], \quad (9)$$

where $\theta_l = 225 \pm 50°K$, $\alpha = 4.2$, and $m^* = 1.4$ m. In view of the similarity of the monoclinic-triclinic crystal structures and the similar values of n, the factor of 2.5 decrease in the vibrational frequency of the pertinent optical mode seems unlikely. It would be more probable that along with an approximately 565°K optical mode the electrons in the triclinic phase are affected by an additional scattering mechanism. At these temperatures scattering by ionized impurities (*53*) or neutral impurities (*54*) can be eliminated since the calculated mobilities are over ten times higher than the observed. The scattering of conduction electrons by piezoelectric acoustical phonons (*55*, *56*) leading to $\mu \alpha T^{-1/2}$ is a possibility.

Seebeck Studies on WO_3

In the case of a single conduction band, the electronic contribution to the thermoelectric power

(S_e) can be written (*57*).

$$S_e = -\left|\frac{k}{q}\right|(T_E - \eta), \tag{10}$$

where T_E is an energy transport term. In the case of a band density of states $N_c = 2(2\pi m^* kT/h^2)^{3/2}$ and $\exp(\eta) = n/N_c$ the above expression can be written

$$S_e = -\left|\frac{k}{q}\right|\left\{T_E + \ln\frac{2(2\pi m^* kT)^{3/2}}{nh^3}\right\}. \tag{11}$$

Using $\theta_l = 565°K$, T_E can be calculated from the weak-coupling theory of Howarth-Sondheimer. Figure 9 shows the course of the observed Seebeck coefficient in the monoclinic phase as compared to that calculated using the rigid band mass and the polaron mass. The experimental data not only do not agree in magnitude but have the reverse temperature dependence. One possibility is that the polaron band mass increases (*45*, *58*) as the temperature is lowered. However, in order to account for the slope of the data, m^{**} would have to increase by a factor of 3 as the temperature is lowered from 450 to 300°K. This is not likely. Another possibility is that the Howarth–Sondheimer weak-coupling treatment does not apply (since $\alpha = 3$) and, therefore, the transport term cannot be calculated within that framework. This may be true, but T_E would have to be so strongly dependent on temperature (increasing from 2.9 at 450°K to 4.4 at 300°K) that this possibility is unlikely. It would seem that a contribution other than that given by Eq. (11) is present.

Below room temperature, the observed Seebeck data are given in Figs. 10 and 11 for the nearly untwinned and the highly twinned WO_3 crystals, respectively. The two crystals have Seebeck coefficients that are similar in magnitude, but the transitions shown in Fig. 11 are not sharp because of the extensive twinning in the original crystal. The solid curve at the top of Fig. 10 is the expected S_e if only changes in n are considered as the temperature is lowered, assuming optical-mode scattering ($\theta_l = 565°K$) and $m^{**} = 3.26$ m. In both the magnitude and the temperature dependence the experimental data deviate from the simple theory. An additional contribution to S_e must be present in all the phases. Although strong coupling to piezoelectric acoustical phonons could account for the enhanced Seebeck voltage in the triclinic and low-temperature phases, the difference in the centrosymmetric monoclinic phase cannot be explained on this basis. Rather, it appears there must be an appreciable phonon drag term (S_{pd}) arising from the preferential scattering of electrons by the phonon current. In semiconductors S_{pd} has been experimentally linked to the coupling of electrons to acoustical modes by nonpolar (*59*) or polar (*56*) interactions if the crystal is piezoelectric. Phonon drag is indicated if there appears a peak in the observed thermoelectric power along with no anomalies in the carrier concentration over some

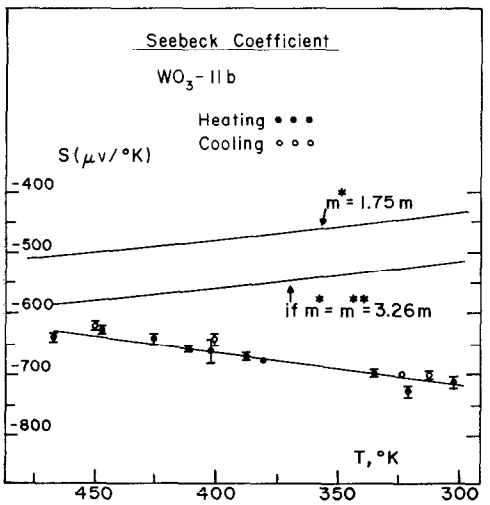

FIG. 9. Seebeck coefficient versus temperature for a single crystal of WO_3. The two upper curves are calculated ones using rigid band mass and polaron mass, respectively.

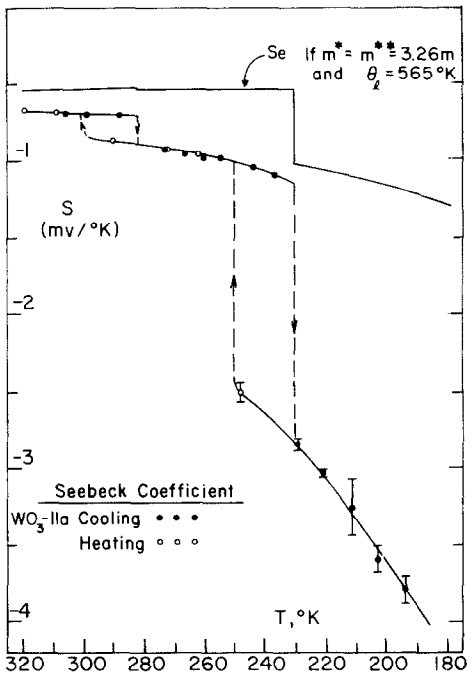

FIG. 10. Seebeck coefficient versus temperature for a single crystal of WO_3 containing some (100) twin planes at the ends. Uppermost curve is calculated without phonon drag.

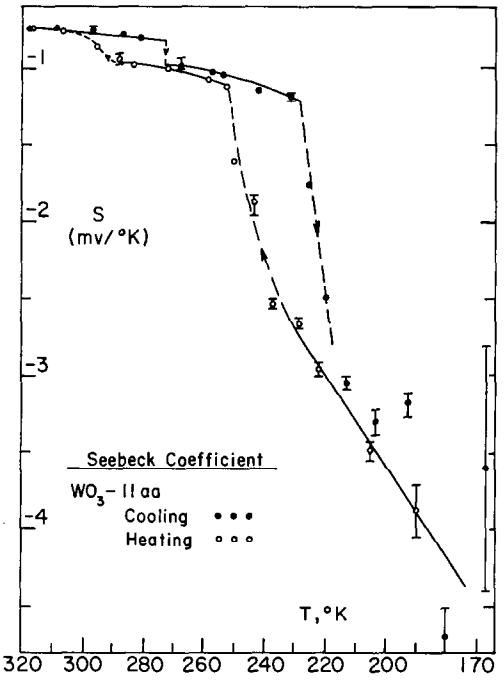

FIG. 11. Seebeck coefficient versus temperature for a single crystal of WO_3 with extensive (100) twinning along its entire length.

temperature interval. For a nondegenerate semiconductor the decrease in S_{pd} from its maximum value on heating has been given by Herring (*59*)

$$S_{pd} = f_r \tau_p c_s^2 / \mu_D T, \tag{12}$$

where f_r indicates the fraction of total available momentum interchanged with acoustical phonons, μ_D is the carrier drift mobility, c_s is the sound velocity, and τ_p is the phonon relaxation time. In general, for long-wavelength acoustical phonons $\tau_p \sim Q^{-s} T^{s-5}$, where Q is the phonon wave vector and s is a parameter which depends on the crystal structure (*60*). For cubic crystals $s = 2$ for long wavelengths; therefore, τ_p varies as T^{-4} since $(Q)^2 \sim T$. In the acoustic scattering range μ_D varies as $T^{-3/2}$ so that S_{pd} should decrease from its maximum value as $T^{-3.5}$. Equation (12) is valid for small n; as n increases τ_p and, therefore, S_{pd} decrease.

Recently it has been suggested (*61*, *62*, *63*) that an optical phonon drag (opd) exists and that its contribution to the total thermoelectric power may be larger than S_e at temperatures where S_{pd} is negligible. Plăvitu (*61*, *62*) has derived expressions for S_{opd} for the case where the optical-phonon relaxation time, $(\tau_p)_0$, varies as $(Q)_0^{-s_0}$, where $s_0 = 0$ to 2. For $\theta_l \gg T$ the temperature dependence can be written

$$S_{opd} \sim \frac{\exp(\theta_l/T)(\tau_p)_0}{\mu_D}. \tag{13}$$

If optical phonon drag exists in the monoclinic phase, this proportionality can be used to obtain the temperature dependence of $(\tau_p)_0$. Using $\theta_l = 565°K$, $\mu_D = \mu_H$, and $S_{opd} = S - S_e$, where S_e is calculated for $m^{**} = 3.26$ m log plots of $S_{opd}\ \mu_D/\exp(\theta_l/T)$ vs T show that $(\tau_p)_0$ varies from T^{-2} to T^{-4} as T increases. Although the temperature dependence of $(\tau_p)_0$ is not known for optical phonons, it has been suggested (*63*) that something like the acoustical case—i.e. $(\tau_p)_0 \sim (Q)_0^{-s_0} T^{s_0-5}$—may hold. If such is the case and $(Q)^2 \sim T$, then s_0 becomes 4 ± 2. This value compares favorably to that which is expected for long-wavelength acoustical phonons in the monoclinic and triclinic systems, where s can be as large as 3 or 4.

The hypothesis that an optical phonon drag is superimposed on S_e could also be extended to the triclinic and low-temperature phases of WO_3. The increase in the magnitude of the measured Seebeck coefficient at the monoclinic-triclinic transition would then be due to a decrease in the optical-mode mobility. To account for the temperature dependence of the mobility in the triclinic phase, θ_l would have to decrease; otherwise, piezoelectric scattering would be indicated. The large increase in S at the triclinic (low temperature) transition is most likely due to a large decrease in n.

A peak in the Seebeck coefficient in the low-temperature phase between 190 and 250°K has not been detected in this investigation; however, Crowder (*51*) found that S begins to decrease with decreasing temperature at about 150°K, which is further evidence that phonon drag does exist in this phase.

Resistivity of WO_{3-x}

Table II summarizes the annealing conditions and compositions assigned to the oxygen-deficient crystals for which measurements are reported below. Figures 12, 13, and 14 show the specific resistivity in the monoclinic phase for these crystals as a function of reciprocal temperature above room temperature. Comparison with Fig. 2 shows that as oxygen deficiency increases there is superimposed on the resistivity of tungsten trioxide another one which decreases with increasing temperature. The irreproducibility of the heating and cooling curves, which is largest for crystal 227*b* (Fig. 12), is due to a decrease in carrier concentration that occurs on heating the crystals above about 85°C.

TABLE II

CHARACTERISTICS OF OXYGEN-DEFICIENT CRYSTALS STUDIED

Crystal	Annealing gas	$-\log p_{O_2}$ (atm)	Assigned composition	Twin[a] patterns
227*b*	O_2	0.01	$WO_{2.999925}$ ± 0.000035	*N*
225*a*				
222*b*	O_2	1.11	$WO_{2.99991}$ ± 0.00002	*N*
222*a*				
218*b*	O_2–Ar	3.14	$WO_{2.99980}$ ± 0.00003	*N*
218*a*				
219*b*	O_2–Ar	4.16	$WO_{2.9988}$ ± 0.0001	*N*
219*a*				*N* + a few (100) walls
220*a*	Ar	$> \sim 5$	$WO_{2.998}$	*N* + some (100) walls
223*b*	CO_2–CO	8.1	$WO_{2.9954}$ ± 0.0001	((110)) + (100)
223*a*				
227*ta*	CO_2–CO	10.2	$WO_{2.9877}$ ± 0.0003	((110)) + (100)

[a] *N* refers to the normal alignment of crystals with *a* axis the direction of current.

This decrease in *n* appears to be due to an annealing out of the oxygen defects due to small traces of oxidizing gases present in the Dewar chamber. The surprising thing is that 85°C is a sufficiently high temperature for this process to occur.

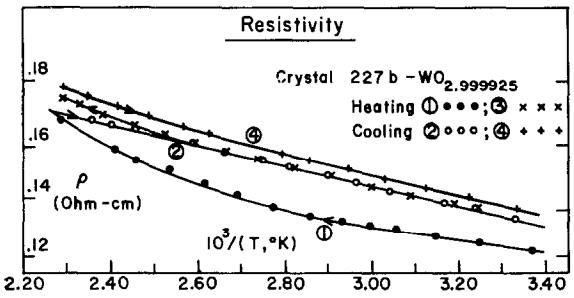

FIG. 12. Resistivity versus reciprocal temperature for single crystal having O/W ratio of 2.999925.

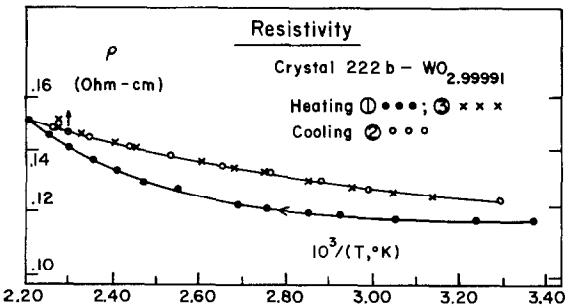

FIG. 13. Resistivity versus reciprocal temperature for single crystal having ratio of 2.99991.

Below room temperature the effect of increasing oxygen removal is shown in the resistivity-reciprocal temperature plots of Figs. 15, 16, and 17. Progressive removal of oxygen pushes both transitions during cooling and heating to temperatures lower than those of the stoichiometric crystals and decreases the magnitudes of the jumps in resistivity at the transitions. The lowest temperature of first appearance of the triclinic phase is about 0°C. The temperature of the triclinic-(low temperature) transition is not appreciably affected until lower

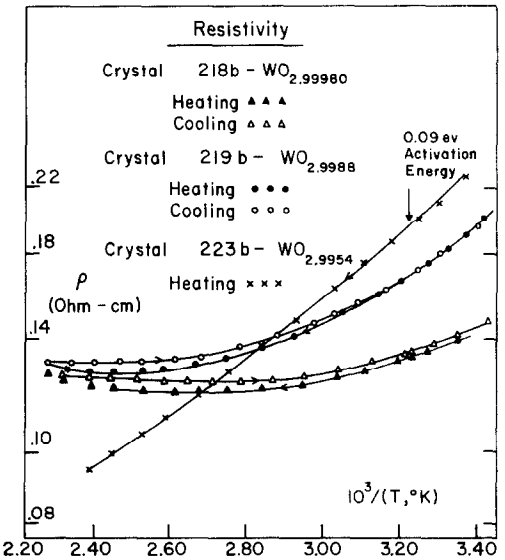

FIG. 14. Resistivity versus reciprocal temperature for single crystals having O/W ratios of 2.99980, 2.9988, and 2.9954.

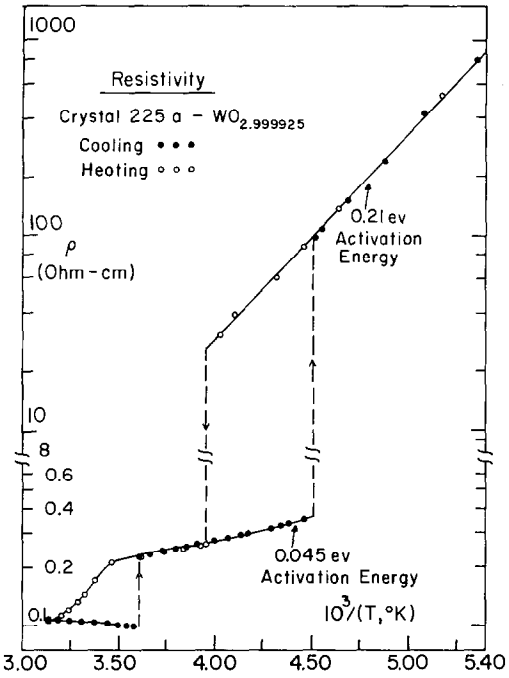

FIG. 15. Resistivity versus reciprocal temperature for single crystal having O/W ratio of 2.999925.

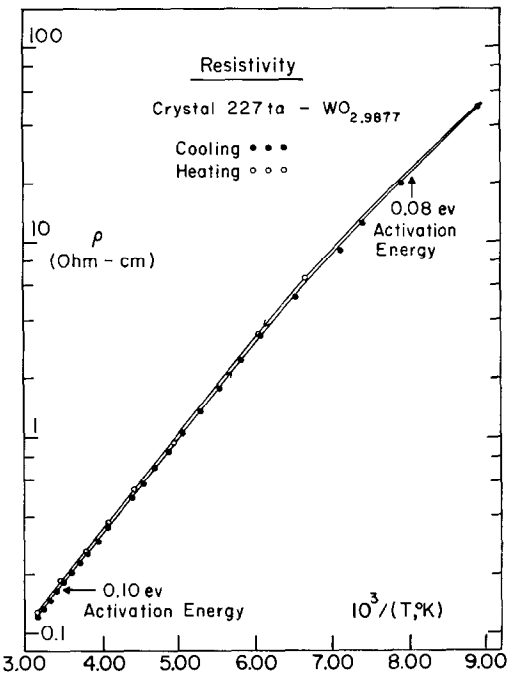

FIG. 17. Resistivity versus reciprocal temperature for single crystal having O/W ratio of 2.9877.

oxygen deficiencies. The lowest temperature of first appearance of the low-temperature phase is 172°K (for crystal 219*a*) or 61°K below that for the stoichiometric oxide (crystal 11*a*). The resistivity bulges shown in Fig. 16 and marked as (ii) and (iii) suggest that the monoclinic-triclinic transition, which occurs in steps, is taking place over a wide temperature interval.

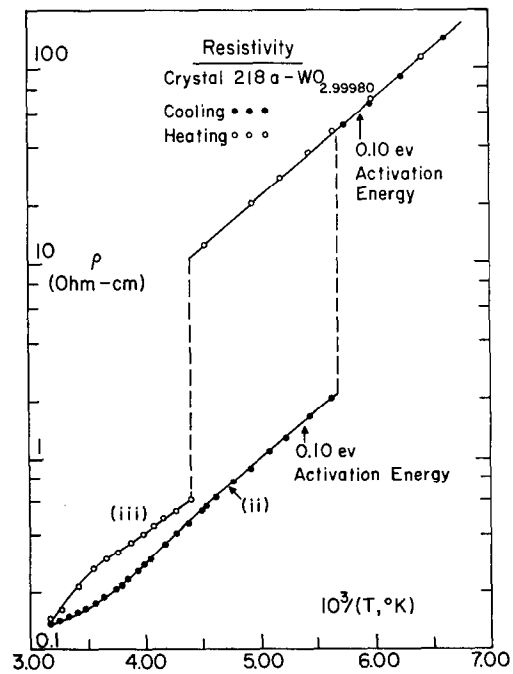

FIG. 16. Resistivity versus reciprocal temperature for single crystal having O/W ratio of 2.99980.

The decrease in the transition temperatures and the step nature of the transitions are understandable on the basis of the constraining effect of the lattice defects. Evidently, the strain associated with these defects must become greater as the crystal cools through the transitions. Assuming other factors constant, successive increases in this contribution to the free energy can be offset if the transition temperatures are lowered in comparison to the case where there are no additional strain terms. The more pronounced effect of oxygen deficiency on the monoclinic-triclinic transition suggests that the difference in free energy between these phases is smaller than that for the triclinic and low-temperature phases.

The activation energy for conduction in the most reduced sample, crystal 227*ta*, is about 0.10 eV. The resistivity in the triclinic phase increases with decreasing temperature faster than with the stoichiometric trioxide. The resistivity still increases with decreasing temperature in the low-temperature phase, but the dependence is not so rapid as for the trioxide. As x increases, the activation energy in the

higher temperature regions of existence of this phase decreases from 0.23 eV (WO_3) to a low of 0.06 eV (crystal 219*a*) and increases slightly to 0.08 eV (crystal 227*ta*). The activation energies just before and after the triclinic-(low temperature) transitions approach each other as x increases.

To a good approximation, it appears that upon reduction of the stoichiometric crystals, another conductivity process is becoming operative over the entire temperature range. The microscopic observation of dark regions separating blocks of yellow trioxide-like material is consistent with the observed resistivities: Superimposed on the resistivity of the stoichiometric oxide (yellow regions) there is another one which decreases as the temperature increases and is attributable to the defect regions.

Hall Studies of WO_{3-x}

The logarithm of the carrier concentration versus the reciprocal temperature for the reduced crystals is shown in Figs. 18, 19, and 20. The signs of the measured Hall voltages indicate that electrons are the majority carriers. Discrete changes in n accompany the monoclinic-triclinic phase transition for crystals 225*a* and 222*a*. Table III summarizes the activation energies for carrier generation and the carrier concentrations at two selected temperatures. In general, as x increases, n increases and the activation energies become greater than for the stoichiometric oxide. There are excellent agreements between crystals annealed under the same conditions, but there are some discrepancies in the trend that activation energy increases as x increases. The maximum available carrier concentration, n_{max}, shown in the last column of Table III was calculated on the basis of two electrons per oxygen atom removed. As can be seen from a comparison of the last two columns, for low values of x, n is greater than n_{max}. In order to explain the difference, additional electrons, most likely arising from donor impurities, would have to be present to the extent of about 5×10^{18}/cc. On the other hand, the analyses may not be sufficiently accurate at low x. For higher values of x, n is less than n_{max}. This is consistent with higher ionization energies for the defects in WO_{3-x} compared to the defects responsible for the electrons in the trioxide.

A basic and as yet unanswered question arises as to the origin of the additional states in the band picture for the oxygen-deficient regions. As noted above, lattice shear and edge sharing of tungsten octahedra take place in these regions. As a result, simple oxygen vacancies are eliminated, and if the

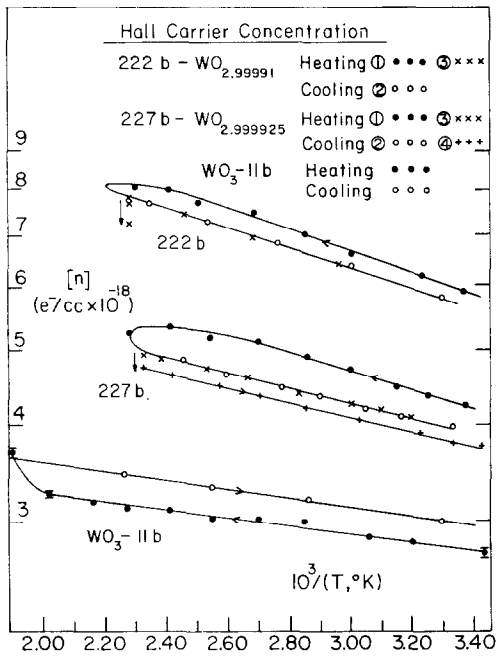

FIG. 18. Hall carrier concentration versus reciprocal temperature above room temperature for two single crystals with O/W ratios of 2.99991 and 2.999925 compared to stoichiometric tungsten trioxide.

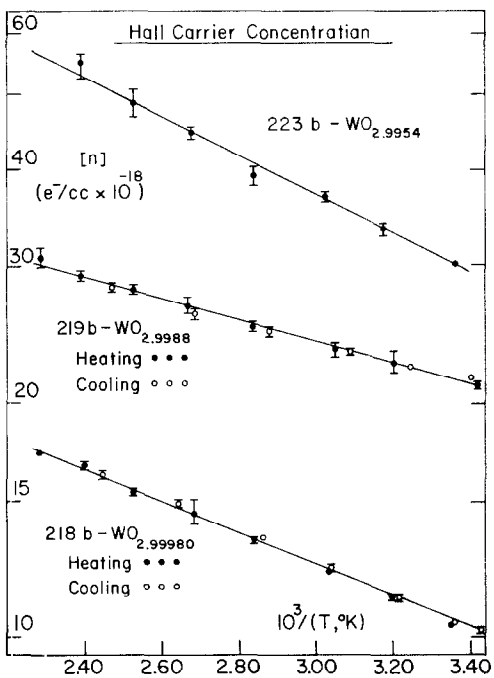

FIG. 19. Hall carrier concentration versus reciprocal temperature above room temperature for single crystals having O/W ratios of 2.99980, 2.9988, and 2.9954.

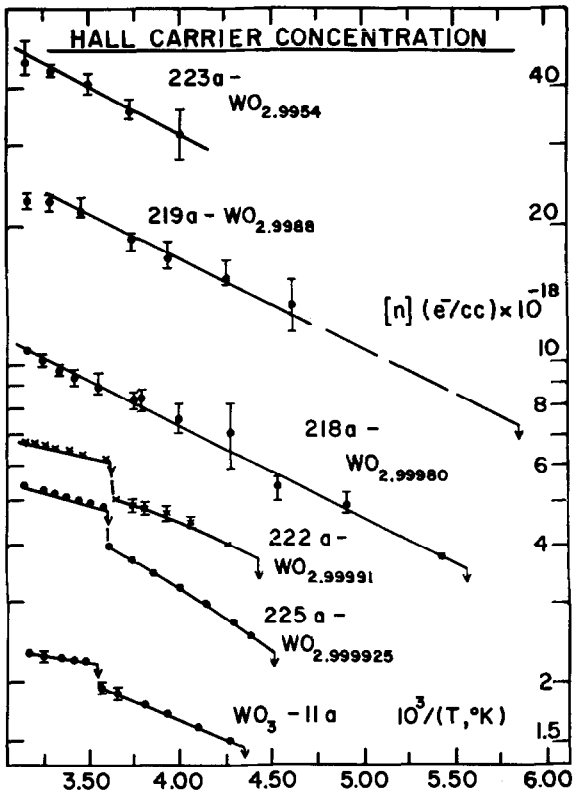

FIG. 20. Hall carrier concentration versus reciprocal temperature below room temperature for various oxygen-deficient single crystals compared to stoichiometric tungsten trioxide.

shear planes are finite, dislocation rings are formed with respect to the unsheared lattice. If oxygen vacancies are eliminated and the Hall measurements for the more reduced crystals indicate that a large fraction of the electrons, although readily accessible with activation energies of 0.03–0.05 eV, are not free, then where are the electrons? A good possibility is that at least some of these electrons are localized at the dislocation rings since these could form acceptor states located well below the conduction-band edge. However, the donors responsible for the electrons in the first place would have to be associated somehow with the edge-sharing octahedra (perhaps as weak W–W bonds) and have energy states closer to the conduction band. Alternatively, the donor levels may have merged with the conduction band, in which case trapping states associated with the dislocations would have to be postulated below the bottom of the conduction band to account for the Hall measurements.

The Hall mobility, which must be considered as some average over the defect and defect-free regions, changes with reciprocal temperature as shown in Figs. 21, 22, 23, and 24. The temperature dependence typical of stoichiometric WO_3 gives way to one that *increases* with temperature as x increases. Furthermore, the magnitude of the mobility at a given temperature decreases as x increases. A clearly recognizable break in the mobility at the monoclinic-triclinic transition is not observed for the more reduced crystals. Table IV summarizes the Hall

TABLE III

HALL CARRIER DATA

Crystal	Activation energy (eV × 100)	Carrier concentration ($e^-/cc \times 10^{-18}$) $T = 318°K$	$T = 417°K$	Calcd.
11*b*	1.10 ± 0.15	2.83	3.1	0
11*a*	1.5 ± 0.4	2.33	—	0
11*aa*	1.6 ± 0.5	2.40	—	0
227*b*	2.35 ± 0.2	4.50	5.5	2.8
225*b*	2.3 ± 0.2	5.42	—	2.8
222*b*	2.8 ± 0.3	6.4	8.1	3.4
222*a*	1.8 ± 0.2	6.7	—	3.4
218*b*	4.1 ± 0.2	11.6	16.5	7.5
218*a*	3.9 ± 0.3	10.7	—	7.5
219*b*	3.1 ± 0.3	24	29	45
219*a*	3.3 ± 0.8	23	—	45
220*a*	—	20	—	75
223*b*	5.0 ± 0.4	34	53	172
223*a*	3.7 ± 1.5	47	—	172
227*ta*	—	110	—	460

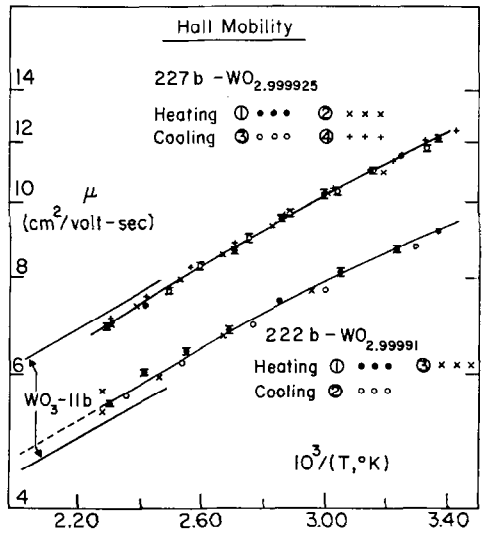

FIG. 21. Hall mobility versus reciprocal temperature for single crystals having O/W ratios of 2.999925 and 2.99991 in the range above room temperature. Stoichiometric WO_3 data shown for comparison.

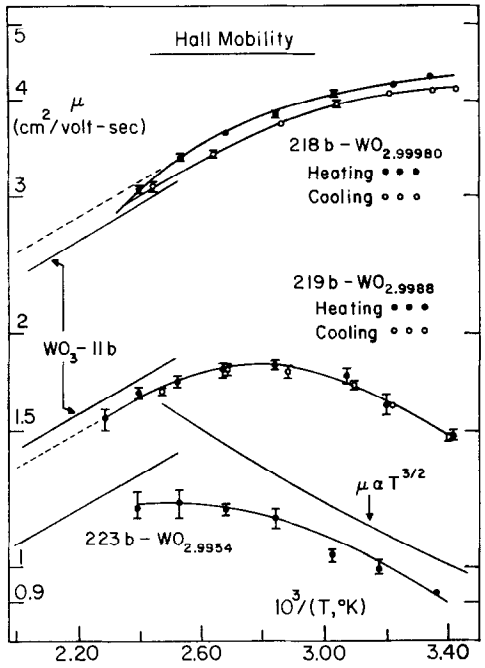

FIG. 22. Hall mobility versus reciprocal temperature for single crystals having O/W ratios of 2.99980, 2.9988, and 2.9954 in the range above room temperature. WO_3 data and $T^{3/2}$ dependence shown for comparison.

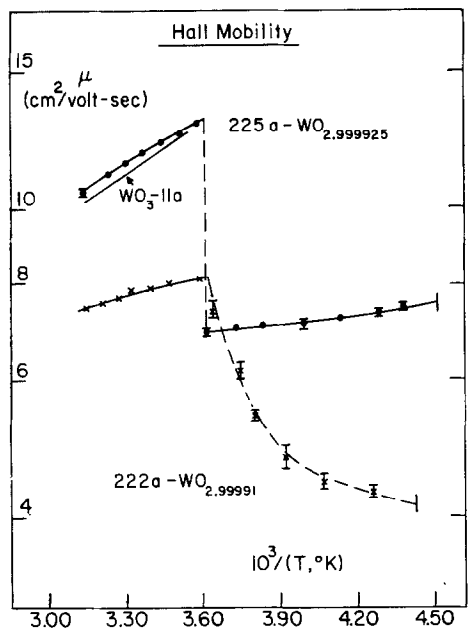

FIG. 23. Hall mobility versus reciprocal temperature for single crystals having O/W ratios of 2.999925 and 2.99991 in the range below room temperature. WO_3 data shown for comparison.

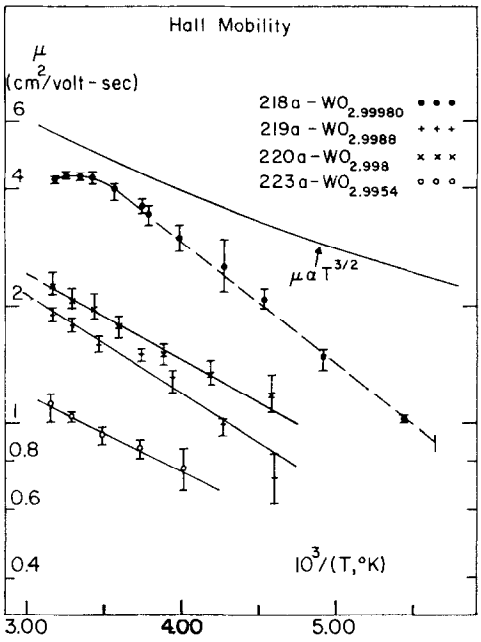

FIG. 24. Hall mobility versus reciprocal temperature for various oxygen-deficient crystals below room temperature. $T^{3/2}$ dependence shown for comparison.

parameters and compares them to those for WO_3. The mobility due to the defect regions increases at least as fast as $\exp(-0.035/kT)$ or $T^{3/2}$. The actual temperature dependence may be stronger than this since polar scattering is contributing to the observed mobility at room temperature and above and there is considerable error in the mobility measurements at low temperatures.

The presence of a high concentration of electrons in WO_{3-x} suggests that there exist similar concentrations of charged donors which act as scattering centers. Assuming that donors are point defects distributed at random, a Hall mobility that varies as $\sim T^{3/2}$ can be attributed (*53*) to the scattering of charge carriers by ionized impurities. Using the procedure outlined by Mansfield (*64*), we find for crystal 223*a*, for example, an ionized-impurity mobility of 2.5×10^4 cm²/V sec assuming a static dielectric constant and 45 cm²/V sec if an effective dielectric constant is used. In either case, the values are high compared to the experimental value of 1.1 cm²/V sec.

Anomalous scattering of charge carriers has been observed in the case of neutron-irradiated semiconductors such as *n*-Ge (*65*), *n*-Si (*66*, *67*), and *n*-GaAs (*68*). In *n*-Ge, for example, neutron irradiation produces islands of *p*-type disordered regions in an *n*-type matrix, and a space charge region is

TABLE IV

HALL MOBILITY DATA

Crystal	x in WO_{3-x}	μ_H at 318°K (cm²/V sec)	ΔE_μ in $\mu \sim \exp(-\Delta E_\mu/kT)$	m in $\mu \sim T^{+m}$
11*b*	0	11.1	—	—
11*a*	0	10.2	—	—
11*aa*	0	13.8	—	—
227*b*	7.5×10^{-5}	11.0	—	—
225*a*	7.5×10^{-5}	10.7	—	—
222*b*	9×10^{-5}	8.4	—	—
222*a*	9×10^{-5}	7.5	—	—
218*b*	2×10^{-4}	4.1	—	—
218*a*	2×10^{-4}	4.2	0.06	3.2
219*b*	1.2×10^{-3}	1.7	0.035	1.5
219*a*	1.2×10^{-3}	2.0	0.05	2.2
220*a*	2×10^{-3}	2.25	0.045	1.8
223*b*	4.6×10^{-3}	1.0	0.035	1.5
223*a*	4.6×10^{-3}	1.1	0.040	1.7
227*ta*	1.23×10^{-2}	0.5	—	—

created that may extend into the crystal bulk (*69*). If the defect regions are sufficiently large, these can act to reduce the electron mobility. However, the anomalous temperature dependence of the mobility cannot be explained on this model. Sonder (*67*) has postulated a model for *n*-Si in which the space charges associated with the large cluster defects scatter electrons in an anomalous fashion at low temperatures. However, for these semiconductors the Hall effect was reported to increase in magnitude on increasing exposure to neutrons; in WO_{3-x}, the Hall effect decreases on introduction of more oxygen deficiency. In other words, the donor nature of the defects is indicated and *p–n* junctions are not expected for WO_{3-x}. Nevertheless, there is in WO_{3-x} the possibility of n^+–*n* junctions (*70*) that come about as follows: Let the reduced crystal be divided into defect (oxygen-deficient) and stoichiometric regions and let the oxygen defects and impurities in the respective regions be distributed at random. If a conduction band similar to that in the stoichiometric region also exists in the defect regions, then the electron concentration (n^+) in the conduction band of a defect region will be greater than that (n^-) in a trioxide-like region. This would lead to a difference in the position of the Fermi level with respect to the bottom of the conduction band in each of the regions and a flow of electrons from the defect to the stoichiometric regions. There would then be an electric field across each boundary which could scatter the charge carriers.

Within the defect regions, transport need not occur only in a conduction band based on tungsten orbitals but may also involve impurity states. If the impurities are sufficiently close that their wave functions overlap, a set of closely spaced states (impurity band) is formed in the energy gap. Carrier mobility associated with such an impurity band is usually considered small in comparison to that in the conduction or valence bands. At low-impurity concentrations band states do not exist, but conductivity can still take place by way of hopping of carriers from one impurity site to a vacant one. The mobility of the hopping process is necessarily thermally activated and its magnitude is also generally considered small compared to that in conduction or valence bands. If the defects in the oxygen-deficient regions are small disks of shear, these could introduce levels into the band gap, and a hopping mode would be a feasible addition to the band behavior. It is difficult, however, to account for the observed maxima in the mobilities of Fig. 22 along with the excellent linearity of the Hall plots of Fig. 19 by such a model.

The mobility maximum can be explained if it is assumed that band processes do not occur in parts of the defect regions. According to Mott (*71*) and Mott and Allgaier (*72*) fluctuations in density or composition associated with disordered lattices can introduce localized states into the energy gap or replace band states with localized states above the bottom of the conduction band. If the disorder is large, there may result a reduction or even elimination of band states in the physically accessible range of energies available to the electrons. In such case the excess electrons would occupy these localized

states, and conduction could take place only by way of phonon-activated hopping processes between levels. This hopping mode would then exist in series with the band behavior associated with neighboring more perfect regions. Depending on the temperature and value of x, each region would contribute in a complex way to the total measured mobility. At low temperatures the observed mobility would be limited by the hopping process; at high temperatures band behavior would take over so as to produce a maximum in the mobility at some intermediate temperature. As x increases, the overall measured mobility would drop because the contribution of the lower-mobility hopping process increases. An important feature of this hopping mechanism is that it is consistent with the idea that there is little change in the activation energy for carrier generation and carrier concentration across the triclinic-(low temperature) transition for the more reduced crystals.

Seebeck Coefficient of WO_{3-x}

Figures 25, 26, 27, and 28 give the Seebeck coefficient data as a function of temperature for various crystals. Table V gives the various Seebeck parameters at 318°K. In general, over the entire temperature range of measurement the absolute value of the measured Seebeck coefficient drops as x increases.

In the monoclinic phase above room temperature the characteristic dependence of the trioxide is replaced by one that is essentially independent of temperature. The next-to-last column of Table V lists S_e, which was calculated by using Eq. (10) at 318°K, assuming that $m^{**} = 3.26$ m, the carriers are distributed at random, and the main scattering of the electrons is by optical-mode lattice vibrations for which T_E from the nondegenerate treatment of Howarth–Sondheimer is 2.01. The agreement between calculated and measured values is poor. If all the calculated values are normalized to that of WO_3–11*b* by adding a constant S_{opd} of -180 μV/°K it can be seen that as x increases the magnitude of the calculated Seebeck coefficients becomes higher than the measured values. Several explanations for this behavior are possible: (1) m^{**} decreases, (2) T_E decreases, or (3) S_{opd} decreases.

(1) That m^{**} decreases is not indicated at all in the mobility data; if anything, m^{**} should increase.

(2) That T_E changes is a good possibility, but that it decreases is unlikely. If ionized-impurity scattering predominates, T_E should increase (*57*) to about 4. Using this value of T_E and 3.26 m for m^*, S_e for heavily reduced crystals 223*b* and 227*ta* comes out to -376 and -282 μV/°K, still higher than the

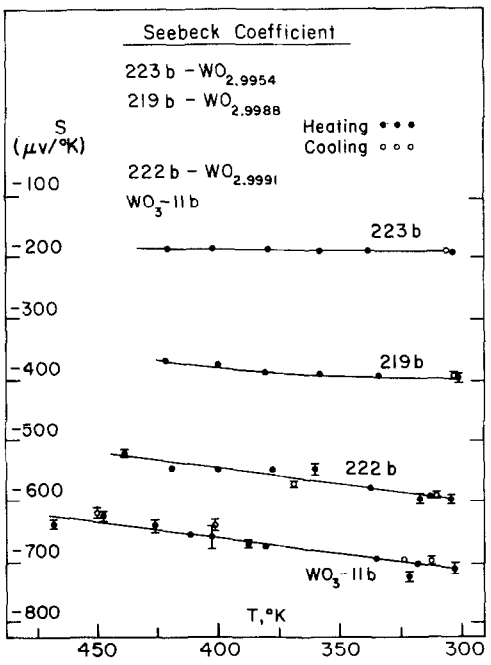

FIG. 25. Seebeck coefficient versus temperature for single crystals of various O/W ratio in the monoclinic phase above room temperature.

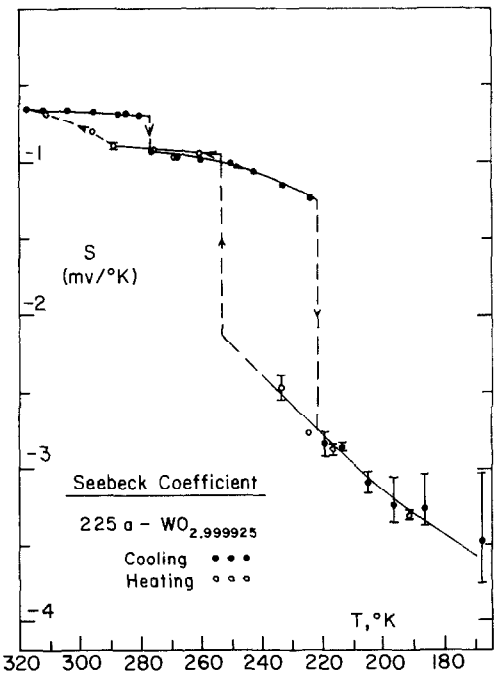

FIG. 26. Seebeck coefficient versus temperature for single crystal with O/W ratio equal to 2.999925.

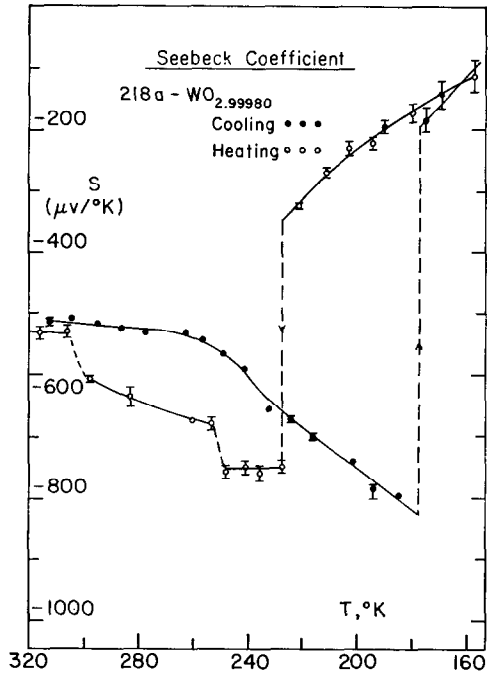

FIG. 27. Seebeck coefficient versus temperature for single crystal with O/W ratio equal to 2.99980.

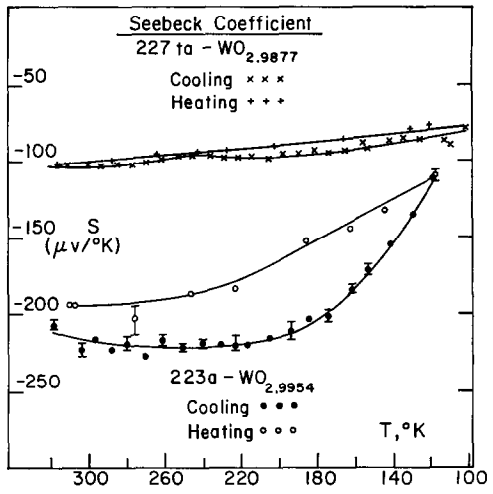

FIG. 28. Seebeck coefficient versus temperature for single crystals with O/W ratio equal to 2.9954 and 2.9877.

experimental values. This would tend to rule out impurity scattering as an important mechanism. For a small-polaron hopping mechanism it is believed that T_E should decrease close to zero. The last column of Table V lists the difference between the experimental thermoelectric power and the Fermi-level contribution to S_e.

$$S - \left|\frac{k}{q}\right| \eta = -\left|\frac{k}{q}\right| T_E + S_{\text{opd}}. \qquad (14)$$

As x increases, the magnitude of the phonon drag plus transport energy terms is seen to decrease.

(3) S_{opd} would be expected to decrease to zero as n increases (saturation effect) and as the concentration of defects increases (increased scattering of phonons by defects). If this is the case, then the transport energy term should also approach zero.

Below room temperature the behavior of the Seebeck coefficient is complicated. Discrete changes in S are evident at each of the sharply defined phase transitions. The monoclinic-triclinic transition in crystal 222*a* occurs in at least two steps: one at 275°K and another at 239°K. (The latter jump was not recorded in the resistivity, which suggests that a phase transition occurred outside that part of the crystal enclosed by the resistivity probes.) No sharp changes in S are evident for the more reduced crystals; this agrees with the smooth resistivity curves. The decrease in the magnitude of S at the triclinic-(low temperature) transition, as well as the decreasing S with decreasing temperature in the low-temperature phase, is very surprising and not understood. Presumably, the phonon-drag contribution is reduced in both phases by the presence of an increased n and/or by increased phonon–defect interactions which scatter long-wavelength optical phonons. Hence, S for both phases should approach S_e as x increases. Since the difference in n across this transition approaches zero with increasing x, there should not be such a large difference between the values of S in the triclinic and low-temperature phases.

Studies on $W_{20}O_{58}$

Crystals were grown by the direct method. Rotation photographs about the *b*-axis were similar to those reported by Magnéli (*6*) in that the reflections were arranged in doublets and triplets along the layer lines, the separations between layer lines correspond to a *b* translational period of 3.77 ± 0.01 Å, and the intensity of the spots corresponding to *h*0*l*, *h*1*l*, and *h*2*l* decreased as *k* increased, but many additional spots, which were mostly of low intensity and could not be attributed to either WO_3 or $W_{18}O_{49}$, appeared along these layer lines and a few of the spots exhibited lower-intensity daughter reflections corresponding to a repeat distance of 27.8 ± 0.9 Å. It may be that there is a superstructure in the *b* direction like that proposed by Magnéli in the *a* and *c* directions due to short W–W distances at the octahedral edge sharing. Batch analyses of crystals gave the composition $WO_{2.895\pm0.002}$ which was slightly more oxygen deficient than expected.

TABLE V

SEEBECK-COEFFICIENT DATA OF WO_3 AND WO_{3-x} AT 318°K

Crystal	x in WO_{3-x}	$S(\mu V/°K)$	$S_e(\mu V/°K)$	$S_{opd} - \left\|\frac{k}{q}\right\| T_E$
11*b*	0	-700 ± 15	-521	-352
11*a*	0	-680 ± 15	-535	-315
11*aa*	0	-750 ± 10	-531	-387
227*b*	7.5×10^{-5}	-660 ± 20	-481	-352
225*a*	7.5×10^{-5}	-650 ± 15	-464	-359
222*b*	9×10^{-5}	-590 ± 10	-451	-312
222*a*	9×10^{-5}	-575 ± 15	-446	-302
218*b*	2.0×10^{-4}	-530 ± 10	-397	-306
218*a*	2.0×10^{-4}	-515 ± 10	-404	-284
219*b*	1.2×10^{-3}	-395 ± 5	-332	-236
219*a*	1.2×10^{-3}	-395 ± 5	-336	-232
220*a*	2×10^{-3}(?)	-402 ± 5	-348	-227
223*b*	4.6×10^{-3}	-193 ± 3	-301	-65
223*a*	4.6×10^{-3}	-207 ± 3	-269	-111
227*ta*	1.23×10^{-2}	-102 ± 2	-185	-90

The resistivity–temperature plot, which was examined from 330 down to 80°K shows a broad maximum at about 270°K and then a slow linear decrease to lower temperatures. At 80°K the specific resistivity was about 500 $\mu\Omega$ cm. The expected concentration of carriers for $WO_{2.895}$ is 4×10^{21}/cc, but this could not be verified by the measurement of a Hall voltage. The thermoelectric power was negative, indicating electrons to be majority carriers, and varied slightly from -15 μV/°C at 90°K to a fairly flat value of -30 μV/°C in the range 240–320°K.

No simple theoretical fit to the data could be arrived at using the various WO_3 parameters suggested above. The general impression is that of metallic behavior with a suggestion of increasing carrier concentration in the higher temperature range.

Magnetic Susceptibility

Tungsten trioxide has a diamagnetic molar susceptibility of $-21.0 \pm 1.7 \times 10^{-6}$ at room temperature (*73*). A powder sample of composition $WO_{2.9875 \pm 0.003}$ showed essentially this same value from 292 to 77.6°K. Below liquid-nitrogen temperature there was a slight decrease in the diamagnetism, eventually switching to a feeble paramagnetism of $+10 \times 10^{-6}$ cgs units per mole at 1.28°K. Although the 0.04-eV carrier generation energy, as determined by Hall studies on crystals of similar composition, suggested the possibility of a large positive contribution to the total susceptibility by trapped localized electrons, there was no magnetic evidence of such unpaired electrons associated with the oxygen deficiency. The behavior at liquid-helium temperatures could be attributable to trace ferromagnetic impurities.

DTA Studies

The general appearance of the WO_3 temperature–time traces was that of an abrupt rise followed by a slower decay to the base line. Since this type of curve is typical of first-order phase transitions, the transitions in WO_3 are so classified. One surprising result was that the triclinic-to-monoclinic transition was not detected in the DTA measurements. Presumably, it takes place in many steps over so wide a temperature interval that the small heat effects are lost in the dynamic measurements. Table VI summarizes the WO_3 data for temperatures and heats of transition as a function of crystal size and thermal history. Although slight increases in T_t are frequent upon recycling the temperature for a given crystal, there are no trends between crystals. Repeated heating and cooling have the tendency to break up single peaks associated with the monoclinic-triclinic transition. So far as the trends in transition heat are concerned, there is a dependence on crystal weight attributable to an external conduction path. The results for the 49-μg crystal are considered to be the most accurate. The magnitudes of the transition heats are very low: 20 cal/mole and 39 cal/mole for the monoclinic-triclinic and triclinic-(low temperature) transitions respectively. The corresponding transition entropies are 0.07 e.u. and 0.16 e.u. These low values are typical of transitions that are not of the order-disorder type (*74*). Their magnitudes are similar to the displacive first-

TABLE VI

DTA DATA ON SINGLE CRYSTALS OF WO_3

Transition	Transition temperature (°C) 49 μg	116 μg	248 μg	330 μg	Transition heat (cal/mole) 49 μg	116 μg	248 μg	330 μg
Monoclinic-to-triclinic								
first cooling	8.4	7.5	9.9	8.4	20.4	15.8	12.5	13.5
second cooling	—	—	15	—	—	—	—	—
third cooling	—	—	13	—	—	—	15.4	—
Triclinic-(low temperature)								
first cooling	−43.6	−48.1	−42.7	−46	39.4	32.3	30.2	27.0
second cooling	−42.6	−46.9	−39.5	−40.2	39.3	31.5	27.8	27.1
third cooling	—	—	−41.9	—	—	—	28.9	—
(Low temperature)-triclinic								
first heating	−21.6	−22.1	−23.1	−24.6	35.9	29.6	28.1	26.4
second heating	−22.1	−23.9	−24.2	−22.0	36.8	30.8	27.8	27.1
third heating	—	—	−23.9	—	—	—	28.7	—

order transitions in $BaTiO_3$. Calibration experiments on a 149-μg crystal of $BaTiO_3$ give 27.8 cal/mole at 4.7°C and 17.5 cal/mole at −89.4°C, in good agreement with previously reported results on much larger samples.

Table VII gives the DTA results for three reduced crystals having O/W ratios of 2.99991, 2.99980, and 2.9988. Except for the last crystal, the transition temperatures on first cooling and heating agree very well with the corresponding resistivity data. On repeated cyclings all gave transition temperatures that were higher than on first cycling. During the heating cycles, peaks were frequently multiple introducing considerable ambiguity in the measured heats.

Due to the size effect in the DTA measurements, comparisons need to be made on the basis of similar-weight crystals. Crystal 222A, weight 306 μg, gave transition heats of 8.5 and 28 cal/mole, comparing favorably with the 13.5 and 26 cal/mole observed for the 330-μg crystal of WO_3. Similarly, the 94-μg crystal 218A gave a heat of about 30 cal/mole, thus comparing to the 30–32 value of the 116-μg crystal of WO_3. Crystal 219A had a weight of 461 μg. The results for the WO_{3-x} crystals fit in rather well compared to the WO_3 crystals. The important conclusion is that the triclinic-(low temperature) transition in the reduced materials is accompanied by essentially the same heat exchange per mole as in the stoichiometric material.

TABLE VII

DTA DATA ON SINGLE CRYSTALS OF OXYGEN-DEFICIENT TUNGSTEN TRIOXIDE

Transition	Transition temperature (°C) 222A $WO_{2.99991}$	218A $WO_{2.99980}$	219A $WO_{2.9988}$	Transition heat (cal/mole) 222A	218A	219A
Monoclinic-triclinic						
first cooling	1.9–1.5	none	none	8.5	none	none
second cooling	6.1–1.7	none	none	6.4	none	none
Triclinic-(low temperature)						
first cooling	−43.5	−99.5	−74.9	27.9	36.2	25.2
second cooling	−48	−63.7	−54.1	28.2	—	23.8
third cooling	−38.1	−59.8	—	—	—	—
fourth cooling	—	−57	—	—	—	—
(Low temperature)-triclinic						
first heating	−28.6	−47	−46.4	20.7	15.7	21.6
second heating	−26.7	−41	−43	—	18.0	—
third heating	−26.1	−43.6	—	28.1	18.9	—
fourth heating	—	−31.4	—	—	28.1	—

References

1. S. Sawada and G. C. Danielson, *Phys. Rev.* **113**, 803 (1959); **113**, 1005 (1959).
2. B. L. Crowder and M. J. Sienko, *J. Chem. Phys.* **38**, 1576 (1963).
3. D. Howarth and E. Sondheimer, *Proc. Roy. Soc. London* **A219**, 53 (1953).
4. T. D. Lee, F. E. Low, and D. Pines, *Phys. Rev.* **90**, 297 (1953); F. E. Low and D. Pines, *Phys. Rev.* **91**, 193 (1953); *Phys. Rev.* **98**, 414 (1955).
5. A. Magnéli, *Ark. Kemi Mineral. Geol.* **24A**, No. 2 (1946).
6. A. Magnéli, *Ark. Kemi* **1**, 513 (1949).
7. A. Magnéli, *Acta Cryst.* **6**, 495 (1953).
8. A. D. Wadsley, *Rev. Pure Appl. Chem.* **5**, 165 (1955).
9. P. Gadó and L. Imre, *Acta Chim. Acad. Sci. Hung.* **46**, 165 (1965).
10. P. Gadó and A. Magnéli, *Acta Chem. Scand.* **19**, 1514 (1965).
11. E. Gebert and R. J. Ackermann, *Inorg. Chem.* **5**, 136 (1966).
12. O. Glemser and H. Sauer, *Z. Anorg. Chem.* **252**, 144 (1943).
13. G. Hägg and A. Magnéli, *Ark. Kemi, Mineral. Geol.*, **19A**, No. 2 (1944).
14. C. Choain and F. Marion, *C. R. Acad. Sci. Paris* **252**, 3258 (1961); *Chim. Ind.* (Paris), **88**, 483 (1962).
15. K. M. Gorbounova and V. A. Arslambekov, *J. Chim. Phys.* **53**, 871 (1956).
16. E. A. Kellett and S. E. Rogers, *J. Electrochem. Soc.* **110**, 502 (1963).
17. P. Gadó, *Acta Cryst.* **16**, A182 (1963).
18. P. Gadó, *Acta Physiol. Acad. Sci. Hung.* **18**, 111 (1965).
19. J. S. Anderson, *Proc. Chem. Soc. London* 166 (1964).
20. S. Tanisaki, *J. Phys. Soc. Japan* **13**, 363 (1958).
21. A. Duquesnoy and F. Marion, *Bull. Soc. Chim. France* 77 (1964).
22. C. Choain and F. Marion, *Bull. Soc. Chim. France* 212 (1963).
23. J. M. Berak, Ph.D. Dissertation, Cornell University, Ithaca, N.Y., 1969.
24. P. T. Davies, *J. Sci. Instr.* **27**, 338 (1950).
25. J. B. Sohn, Ph.D. Dissertation, Cornell University, Ithaca, N.Y., 1965.
26. P. Chieux, Ph.D. Dissertation, Cornell University, Ithaca, N.Y., 1969.
27. A. Magnéli, G. Andersson, B. Blomberg, and L. Kihlborg, *Anal. Chem.* **24**, 1998 (1952).
28. S. Tanisaki, *J. Phys. Soc. Japan* **15**, 573 (1960).
29. T. Horie and T. Iwai, *J. Phys. Soc. Japan* **16**, 424 (1961).
30. T. Iwai and T. Horie, *J. Phys. Soc. Japan* **17**, 1142 (1962).
31. J. S. Anderson and B. G. Hyde, *Bull. Soc. Chim. France* 1215 (1965).
32. J. S. Anderson and B. G. Hyde, *J. Phys. Chem. Solids*, **28**, 1393 (1967).
33. A. L. Companion and M. Mackin, *J. Chem. Phys.* **42**, 4219 (1965).
34. T. S. Moss, "Optical Properties of Semiconductors," p. 30, Butterworths, London, 1961.
35. V. L. Gurevich, I. G. Lang, and Y. A. Firsov, *Fiz. Tverd. Tela* **4**, 1252, 1962.
36. T. Iwai, *J. Phys. Soc. Japan* **15**, 1596 (1960).
37. J. S. Blakemore, "Semiconductor Statistics," p. 138, Pergamon Press, London 1962.
38. N. F. Mott, *Nuovo Cimento Suppl.* **7**, 312 (1958).
39. M. J. Sienko, "The Alkali Metals," Special Publication No. 22, p. 429, The Chemical Society, London, 1967.
40. B. L. Crowder and M. J. Sienko, *Inorg. Chem.* **4**, 73 (1965).
41. R. L. Petritz and W. W. Scanlon, *Phys. Rev.* **97**, 1620 (1955).
42. A. R. Hutson *in* "Semiconductors" (N. B. Hannay, Ed.), p. 541, Rheinhold Publ. Corp., New York, 1959.
43. H. Fröhlich, H. Pelzer, and S. Zienau, *Phil. Mag.* **41**, 221 (1950).
44. D. C. Langreth, *Phys. Rev.* **137A**, 760 (1965).
45. A. Weijland, *Physica* **32**, 625 (1966).
46. D. C. Langreth and L. P. Kadanoff, *Phys. Rev.* **133A**, 1070 (1964).
47. R. P. Feynmann, *Phys. Rev.* **97**, 660 (1955).
48. T. D. Schultz, *Phys. Rev.* **116**, 526 (1959).
49. Y. Ōsaka, *Progr. Theoret. Phys. (Kyoto)* **25**, 517 (1961).
50. L. P. Kadanoff, *Phys. Rev.* **130**, 1364 (1963).
51. B. L. Crowder, Ph.D. Dissertation, Cornell University, Ithaca, N.Y., 1963.
52. D. C. Langreth, *Phys. Rev.* **159**, 717 (1967).
53. E. Conwell and V. F. Weisskopf, *Phys. Rev.* **77**, 388 (1950).
54. C. Erginsoy. *Phys. Rev.* **79**, 1013 (1950).
55. W. A. Harrison, *Phys. Rev.* **101**, 903 (1956).
56. A. R. Hutson, *J. Appl. Phys.* **32**, 2287 (1961).
57. V. A. Johnson *in* "Progress in Semiconductors," Vol. I, p. 63 (A. F. Gibson, Ed.), John Wiley and Sons, Inc., New York, 1956.
58. T. Yokota, *Busseiron Kenkyu*, No. 69, 137 (1953).
59. C. Herring, *Phys. Rev.* **96**, 1163 (1954).
60. C. Herring, *Phys. Rev.* **95**, 954 (1954).
61. C. N. Plăvitu, *Phys. Status Solidi* **12**, 265 (1965).
62. C. N. Plăvitu, *Phys. Status Solidi* **16**, 69 (1966).
63. L. Georgescu, *Physica* **35**, 107 (1967).
64. R. Mansfield, *Proc. Phys. Soc. London* **B69**, 76 (1956).
65. J. H. Crawford, Jr. and J. W. Cleland, *J. Appl. Phys.* **30**, 1204 (1959).
66. G. K. Wertheim, *Phys. Rev.* **111**, 1500 (1958).
67. E. Sonder, *J. Appl. Phys.* **30**, 1186 (1959).
68. L. W. Ankermann, *Proc. Int. Conf. Semicond. Phys. Prague* **946** (1960).
69. B. R. Gossick, *J. Appl. Phys.* **30**, 1214 (1959).
70. R. A. Smith, "Semiconductors," p. 276, Cambridge University Press, London, 1959.
71. N. F. Mott, *Advan. Phys.* **16**, 49 (1967).
72. N. F. Mott and R. S. Allgaier, *Phys. Status Solidi* **21**, 343 (1967).
73. M. J. Sienko and B. Banerjee, *J. Amer. Chem. Soc.* **83**, 4149 (1961).
74. W. Kanzig, *Solid State Phys.* **4**, 60 (1957).